Implementation, Verification & Validation of Explicit Algebraic Reynolds Stress Model in Isogeometric Analysis

T. Volker

TU Delft Delft University of Technology

Challenge the future

Thesis for the degree of MSc in Marine Technology in the specialization of Ship Hydromechanics

Implementation, Verification & Validation of Explicit Algebraic Reynolds Stress Model in Isogeometric Analysis

By

Thijs-Gerrit Volker

This thesis (MT.21/22.030.M) is classified as confidential in accordance with the general conditions for projects performed by the TUDelft.

20-04-2022

Thesis exam committee
Chair/Responsible Professor: Dr.ir. I. Akkerman
Staff Member: Dr.ir. G.H. Keetels
Staff Member: R.G. Diez Sanhueza MSc.

Author Details
Studynumber: 4432126

Contents

1 Thesis Objective **5**
- 1.1 Rounded Transom Interceptor . . . 6
- 1.2 Goal . . . 6
- 1.3 Outline . . . 7

2 Turbulence Modelling **8**
- 2.1 Reynolds Averaged Navier Stokes . . . 8
- 2.2 General Boussinesq Hypothesis . . . 9
- 2.3 Algebraic Expression for Reynolds Stress Anisotropy . . . 9
- 2.4 Explicit Algebraic Reynolds Stress Models . . . 11
  - 2.4.1 Differential Reynolds Stress Models . . . 11
  - 2.4.2 Weak Equilibrium Assumption . . . 11
  - 2.4.3 Explicit Solution . . . 13
- 2.5 Non-Linear Eddy Viscosity Models . . . 14
- 2.6 Validation for Separated Flows . . . 15
- 2.7 Turbulence Model . . . 15
  - 2.7.1 Governing Equations . . . 15
  - 2.7.2 Zonal Coefficients . . . 16
  - 2.7.3 Constitutive Model . . . 16

3 Finite Element Formulation **19**
- 3.1 Approximate Solution . . . 19
- 3.2 Weighted Residual Techniques . . . 20
  - 3.2.1 Point Collocation . . . 20
  - 3.2.2 Subdomain Collocation . . . 21
  - 3.2.3 Galerkin Method . . . 21
- 3.3 Weak Formulations . . . 21
  - 3.3.1 Traditional Formulation . . . 21
  - 3.3.2 Residual Formulation . . . 22
- 3.4 Stabilisation Techniques . . . 23
  - 3.4.1 Streamline-Upwind / Petrov-Galerkin . . . 23
  - 3.4.2 Pressure-Stabilised / Petrov-Galerkin . . . 23
  - 3.4.3 Galerkin Least Squares . . . 24
  - 3.4.4 Variational Multiscale . . . 25
  - 3.4.5 Stabilised System of Equations . . . 26
- 3.5 Discontinuity Capture . . . 27
- 3.6 Boundary Conditions . . . 27

4 Numerical Implementation **29**
- 4.1 Realizability of Turbulence Quantities . . . 29
- 4.2 Production Limiter . . . 30
- 4.3 Solution Procedure . . . 31
  - 4.3.1 Time Integration in DelFi . . . 31
- 4.4 Solution Control . . . 33

5 Numerical Experiments **34**
- 5.1 Grad-Div Stabilisation . . . 34
- 5.2 Homogeneous Isotropic Decaying Turbulence . . . 36
- 5.3 Homogeneous Shear Flow . . . 37
- 5.4 Backward Facing Step . . . 38
  - 5.4.1 Case description . . . 38

5.4.2 Effect of Artificial Diffusion . . . 39
5.4.3 Effect of initial CFL number . . . 42
5.4.4 Validation . . . 44

6 Conclusion **47**
6.1 Recommedations . . . 47

A Transformation of ω Equation **49**
A.1 Convection Term . . . 49
A.2 Diffusion Term . . . 49
A.3 Cross-Diffusion Term . . . 50
A.4 Logarithmic Equation for ω . . . 50

B Weak Form Equations **51**

References **53**

1

Thesis Objective

Computing capabilities have increased tremendously over the last few decades. This enabled the use of computers for engineering design. Nowadays, the use of computer simulations, sometimes referred to as Computer Aided Engineering (CAE), is becoming a common tool in various areas of engineering. As computational power kept increasing, more complex physical phenomena could be tackled by simulation codes. In the field of fluid dynamics, the earliest codes where based on potential flow theory. This evolved to full (incompressible) viscous flow simulations, which are often called Computational Fluid Dynamics (CFD). In turn, more complex phenomena are tackled by CFD, among others: compressible flow, multi-phase flow, combustion and fluid-structure interaction.

An especially challenging part of CFD is the presence of turbulence. Generally, there are three approaches to account for turbulence: Direct Numerical Simulation (DNS), Large Eddy Simulation (LES) and Reynolds Averaged Navier Stokes (RANS). DNS fully resolves turbulence by computing all scales present in the flow. A model for the small scales is introduced in LES, while still resolving large turbulent motion. Lastly, RANS models all turbulent scales. In industrial applications, such as the flow around a ship, LES and DNS are often too computationally expensive. Therefore, RANS is commonly used in industrial applications to account for turbulence.

In RANS, an additional stress-like term appears in the governing equations, which represents turbulence. There are two major approaches to model this term. The first one regards turbulence as a diffusive process and alters the viscosity in the Navier-Stokes equations accordingly. This class of models are the Eddy Viscosity Models (EVM), and generally require two additional differential equations to be solved. The other method, called Reynolds Stress Models (RSM), derives differential equations for each stress component. RSM are more accurate but computationally more expensive and harder to solve than EVM. EVM are the most commonly applied model of RANS as it is less computationally expensive.

EVM are known to fail in more complex flows than the shear flows for which they were designed. Other RANS models have been proposed to improve predictive performance in these complex flows, while remaining about as expensive as EVM. One such type of models are the Explicit Algebraic Reynolds Stress Models (EARSM). These are formally derived from RSM and are functionally similar to EVM. The goal of EARSM is to inherit the accuracy of RSM while solving the same number of differential equations as EVM.

One particular group of complex flows of interest is separated flow, as they are important in many engineering settings. While remaining relatively inexpensive, but with improved accuracy, EARSM appears to be a more suitable candidate than EVM to compute these flows. The performance of EARSM for separated flow has mainly been evaluated for simple configurations, such as periodic hills, diffusers and the backward facing step. Evaluation of practical applications are limited to high-lift aerodynamics, such as a wing-body configuration. This thesis aims to expand this to a maritime application. The application considered is a rounded transom interceptor, as there is currently ongoing research into separation with this configuration.

1.1. Rounded Transom Interceptor

An interceptor is a device that is used for fast ships to control the trim, with the aim to improve sea-keeping behaviour in waves (see Figure 1.1). This is done by vertically lowering a device below the transom. This creates an obstruction in the flow resulting in a stagnation point, which locally increases pressure. This modified pressure distribution generates lift. These classical interceptors are located behind a square transom and are therefore only able to generate lift in one direction.

Experiments with interceptors behind a rounded transom have been carried out, which showed that a negative lift could be attained this way. With lift in both directions, better control of the vessel is possible. In simulations it was shown that this new configuration resulted in lower accelerations in the bow compared to a classical interceptor (Rijkens et al., 2013). This negative lift is likely a result of separation at the rounded transom. Within the separated flow, the pressure is reduced and thus generating negative lift. Currently, experiments are carried out at Delft University of Technology to investigate this region of separated flow.

Figure 1.1: Two transom interceptors mounted to the stern of a vessel. These devices are lowered into the oncoming flow, generating lift by creating a stagnation point. Note the sharp angle between the stern and keel instead of being rounded. Modified image from Rijkens et al. (2011).

1.2. Goal

For the analysis of a rounded transom interceptor, it is beneficial if the effect of separation can be predicted numerically. To this extent, the intent is to validate an Explicit Algebraic Reynolds Stress Model to determine its applicability. As a whole, this thesis is concerned with the implementation, verification and validation of this model. The model is implemented using Isogeometric Analysis. This is a finite element method using NURBS as basis functions. A major benefit is that curved geometries can be represented exactly, such as a rounded transom. A finite element formulation is unstable in convection dominated problems, therefore a stabilised formulation has to be specified and implemented in this work. The overall goal of this thesis is formulated as:

> The goal of this thesis is to implement, verify and validate an Explicit Algebraic Reynolds Stress model, using a stabilised Isogeometric Analysis formulation, for separated flow occurring near a rounded transom interceptor.

This goal leads to four major sub-question categories related to the implementation, performing simulations, validation of physics and the rounded transom interceptor. These categories are formulated as four overarching questions:

- What is an appropriate numerical formulation so that a stable result is obtained without oscillations, over- and undershoot in the solution variables?
- What input (parameters) are required to obtain a converged solution, such as mesh resolution, iteration stopping criteria, time step, etc.?
- How does the implemented Explicit Algebraic Reynolds Stress Model perform in (standard) separation flow test cases, such as 2D periodic hill, asymmetric diffuser and Stratford ramp?

- What are the differences between the numerical result and experimental data for a rounded transom interceptor, for quantities such as skin friction, pressure, Reynolds stress, etc.?

1.3. Outline

The main work in this thesis is to combine turbulence modelling (EARSM) with numerics (Isogeometric Analysis). These topics are important ”pillars” on top which this thesis builds (see Figure 1.2). The outline of this thesis reflects this by first introducing the necessary aspects of turbulence modelling and numerics to implement a numerical method. It then concludes with various numerical experiments.

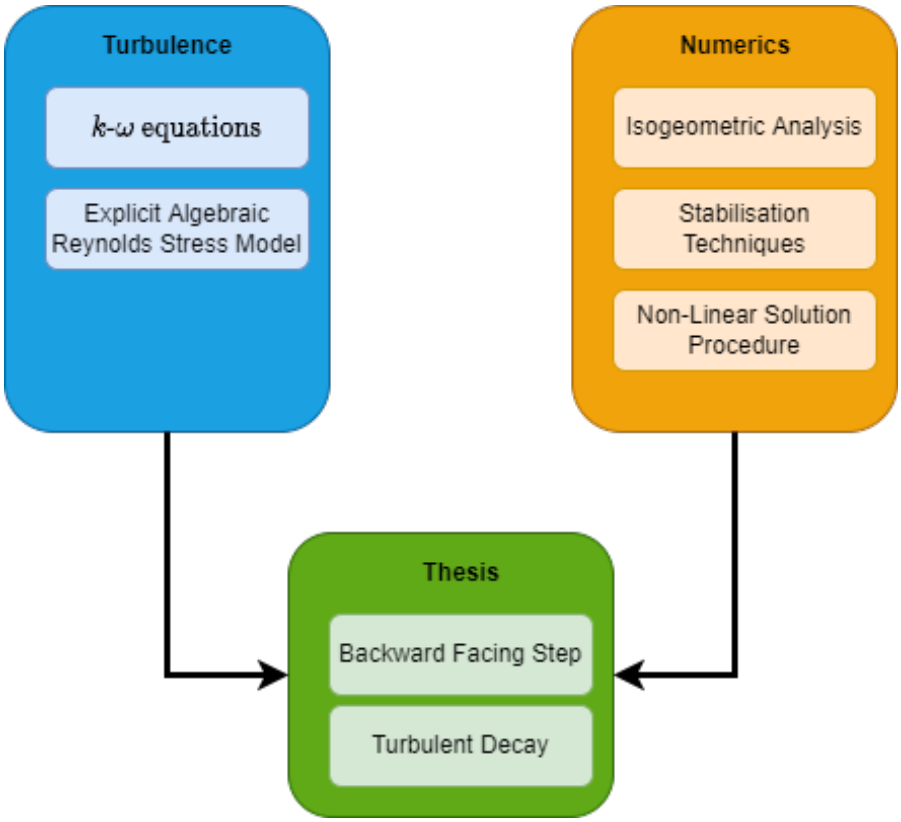

Figure 1.2: Illustration of how this thesis builds on top of turbulence modelling and numerics.

Chapter 2 introduces turbulence modelling. It introduces, very briefly, the Reynolds Averaged Navier-Stokes (RANS) equations. Most of this chapter describes the general derivation procedure for Explicit Algebraic Reynolds Stress Models (EARSM). It concludes with an overview of the turbulent equations and EARSM used in this thesis.

Next, in chapter 3, the first part of numerics is introduced. This chapter describes the Finite Element Method, and in extension thereof Isogeometric Analysis. The chapter starts with a general introduction to the Finite Element Method. The approximation of the solution and derivation of the weak formulation is briefly presented. Afterwards, several stabilisation techniques for fluid flow are presented. The chapter ends with a brief discussion of incoperating boundary conditions in the finite element method.

Chapter 4 describes various aspect that have been used in implementing the numerical method in this thesis. It starts with modifications that are applied to the turbulent equations to satisfy certain realizability constraints and improve robustness. The chapter ends with a description of the solution procedure in the in-house code DelFI.

The performance of the numerical method is investigated in chapter 5. A turbulent decay test is used to evaluate the production and dissipation terms for constant shear. In addition, the backward facing step case is presented to evaluate the perfomance in seperating flows.

Lastly, this thesis concludes with a conclusion and recommedations in chapter 6.

2

Turbulence Modelling

This chapter discusses Explicit Algebraic Reynolds Stress Models (EARSM) and Non-Linear Eddy Viscosity Models (NLEVM) with respect to their applicability to separated flows. First, a brief introduction to the Reynolds Averaged Navier-Stokes Stokes equations is given. The Boussinesq hypothesis is then introduced as a model for the Reynolds stresses. This assumption is the basis for the well-known k-ε and k-ω models. The Boussinesq hypothesis is extended to a more general framework for the algebraic representation of the Reynolds stresses. This framework is then considered as the basis for all EARSM and NLEVM. At this point the (full) Reynolds Stress equations are introduced and the assumptions therein. These equations are the basis of EARSM, and to a lesser extent NLEVM, and influence the predictive capabilities of EARSM. Lastly, the predictive performance of EARSM and NLEVM are reviewed. Various models are compared with experiments, LES/DNS and/or differential Reynolds Stress Models (RSM).

2.1. Reynolds Averaged Navier Stokes

The basic idea of the Reynolds Averaged Navier Stokes (RANS) approach is that the flow can be decomposed into a mean and fluctuating part. For most (industrial) applications the mean values are regarded as time averaged quantities. Strictly speaking, this is only valid in statistically stationary flows. This does not necessarily hold in separated flows. For example, vortex shedding in the wake of a cylinder is not stationary (Durbin & Reif, 2010, Ch. 2.2). For now, the flow is considered stationary. The period over which the averaging is performed is assumed to be sufficiently large compared to the (largest) turbulent time scales. The RANS equations are obtained by substituting the flow decomposition in the Navier-Stokes equations and averaging over all the terms. More detailed explanations may be found in textbooks on turbulence, such as (Nieuwstadt et al., 2016; Pope, 2000). The RANS equations are given by:

$$\frac{\partial \overline{u}_i}{\partial x_i} = 0 \tag{2.1}$$

$$\frac{\partial \overline{u}_i \overline{u}_j}{\partial x_j} = \frac{1}{\rho}\frac{\partial \overline{p}}{\partial x_i} + \frac{\partial}{\partial x_j}\left(\nu\left(\frac{\partial \overline{u}_i}{\partial x_j} + \frac{\partial \overline{u}_j}{\partial x_i}\right)\right) - \frac{\partial \overline{u_i' u_j'}}{\partial x_j} \tag{2.2}$$

Where $\overline{u}_i$ is the mean flow velocity and $\overline{p}$ mean pressure. Fluctuating velocity is denoted by u_i', and $\bar{\cdot}$ is the averaging operation. The material constants ρ and ν are density and kinematic viscosity, respectively. Note that the index notation is used here. Repeated indices in a term, such as in Eq. 2.1, imply summation over $i = \{1, 2\}$ in 2D and $i = \{1, 2, 3\}$ in 3D. The first equation, Eq. 2.1, is recognised as the continuity equation. Eq. 2.2 represents the momentum equations, where the last term is the effect of turbulence on the mean flow field. Within the setting of RANS, this is the term that requires modelling. The tensor $\overline{u_i' u_j'}$ is referred to as the Reynolds stress tensor, and is the focus of turbulence models.

2.2. General Boussinesq Hypothesis

A popular method for approximating the Reynolds stresses is to regard turbulence as an diffusive process, first introduced by Boussinesq. In this model, the Reynolds stresses are linked to the mean flow rate of strain through a turbulent / eddy viscosity ν_T, similar to Stokes' hypothesis for molecular stresses. The formulation for general flows is referred to as the general Boussinesq hypothesis:

$$\overline{u_i' u_j'} = \frac{2}{3} k \delta_{ij} - \nu_T \left(\frac{\partial \overline{u}_i}{\partial x_j} + \frac{\partial \overline{u}_i}{\partial x_i} \right) \tag{2.3}$$

Here, k ($= {}^1\!/_2 \, \overline{u_i' u_i'}$) is the turbulent kinetic energy and δ_{ij} the Kronecker delta. The general Boussinesq hypothesis may be taken in the momentum equations as an effective viscosity and a modified pressure. The pressure $\overline{p}$ is replaced by a modified pressure $\tilde{p}$, in which ${}^2\!/_3 k$ is regarded as a turbulent pressure. Furthermore, viscosity is replaced by an effective viscosity ν_{eff}:

$$\frac{\tilde{p}}{\rho} = \frac{\overline{p}}{\rho} + \frac{2}{3} k \qquad \nu_{eff} = \nu + \nu_{eff} \tag{2.4}$$

The problem of determining the Reynolds stresses is now reduced to determining the turbulent viscosity ν_T. The RANS momentum equations in Eq. 2.2 may now be written as, using Eq. 2.4:

$$\frac{\partial \overline{u}_i}{\partial t} + \frac{\partial \overline{u}_i \overline{u}_j}{\partial x_j} = \frac{1}{\rho} \frac{\partial \tilde{p}}{\partial x_i} + \frac{\partial}{\partial x_j} \left(\nu_{eff} \left(\frac{\partial \overline{u}_i}{\partial x_j} + \frac{\partial \overline{u}_i}{\partial x_i} \right) \right) \tag{2.5}$$

This is the basis for a class of turbulence models which are referred to as Linear Eddy Viscosity Models, or sometimes simply Eddy Viscosity Models (EVM). Nowadays, these models are usually associated with two transport equations for turbulent quantities. Often, these are the turbulent kinetic energy k and turbulent dissipation ε or specific dissipation $\omega = \varepsilon / k$. However, different quantities have been proposed in literature. A notable exception is the Spalart-Allmaras model, which uses a single transport equation for the turbulent viscosity ν_T.

2.3. Algebraic Expression for Reynolds Stress Anisotropy

Two deficiencies are attributed to the eddy viscosity approach. First, it uses a scalar (ν_T) to represent the six unique components of the Reynolds stress tensor. Secondly, the Reynolds stresses are instantaneously coupled to the mean flow gradients. EARSM/NLEVM aim to improve the first deficiency by introducing a non-linear relationship between Reynolds stresses and mean flow gradients. This allows the components of the Reynolds stress tensor to be specified independently.

It is convenient to introduce the Reynolds stress anisotropy. As will become clear later on, turbulence models focus on modelling the anisotropy. EARSM/NLEVM are especially concerned with deriving an appropriate constitutive relationship for the Reynolds stress anisotropy. The Reynolds stress anisotropy is defined as:

$$a_{ij} = \frac{\overline{u_i' u_j'}}{k} - \frac{2}{3} \delta_{ij} \tag{2.6}$$

Note that the anisotropy, as defined here, is a dimensionless quantity. Sometimes, a different definition is used in literature for the anisotropy. This alternate formulation for the anisotropy is defined as:

$$b_{ij} = \frac{\overline{u_i' u_j'}}{2k} - \frac{1}{3} \delta_{ij} = \frac{a_{ij}}{2} \tag{2.7}$$

To better illustrate the relationship between EVM and EARSM/NLEVM later on, the velocity gradient is decomposed in its symmetric and skew-symmetric part. The symmetric part represents the rate-of-strain, whereas the skew-symmetric tensor is the rotation tensor. The dimensionless rate-of-strain tensor is defined as:

$$S_{ij} = \frac{\tau}{2} \left(\frac{\partial \overline{u}_i}{\partial x_j} + \frac{\partial \overline{u}_j}{\partial x_i} \right) \tag{2.8}$$

Similarly, the dimensionless rotation tensor is defined as:

$$\Omega_{ij} = \frac{\tau}{2}\left(\frac{\partial \overline{u}_i}{\partial x_j} - \frac{\partial \overline{u}_j}{\partial x_i}\right) \tag{2.9}$$

Here, τ is a characteristic turbulent time scale that has to be specified. Similar to EVM, EARSM / NLEVM use two additional transport equations, which are used to define τ. Usually, k-ε or k-ω models are used, which are functionally the same as those in EVM. The Boussinesq hypothesis may now be written as:

$$a_{ij} = -\frac{2}{\tau}\frac{\nu_T}{k}S_{ij} \tag{2.10}$$

The Boussinesq hypothesis thus amounts to the assumption that the Reynolds stress anisotropy is linearly related to the mean rate-of-strain. The validity of this assumption is discussed by Pope (2000, Ch. 10). Pope concludes that the linear dependence is reasonable in flows with slowly varying strain rates, such as boundary layers. It is further discussed, however, that it is not valid in general and fails, for example, in strong swirling flows or flows with significant streamline curvature. One may seek to improve this by using a non-linear formulation for a_{ij}. This is the approach undertaken by NLEVM and EARSM.

Following the discussion by Gatski and Jongen (2000), Hellsten and Wallin (2009), a new formulation for a_{ij} is sought as a linear combination of tensors. Since a_{ij} is symmetric and traceless, these tensors also have to be symmetric and traceless, so as not to violate the mathematical properties of a_{ij}. The anisotropy is constructed as:

$$a_{ij} = \sum_n \alpha_n T_{ij}^{(n)} \tag{2.11}$$

At this point, it is assumed that a_{ij} is only dependent on S_{ij}, Ω_{ij} and τ. Thus, the tensors $T_{ij}^{(n)}$ are functions of two kinematic tensors. This approach is pioneered by Pope (1975), who was the first to report, based on the work by Spencer and Rivlin (1958), that only 10 groups can be constructed from S_{ij} and Ω_{ij} which are symmetric and traceless in 3D. This is based on the Caley-Hamilton theorem. It states that, in n dimension, a_{ij}^n is a linear combination of lower powers. For three dimensions this is (Durbin & Reif, 2010, Ch. 2.3):

$$a_{ij}^3 = III_a\delta_{ij} - II_a a_{ij} + I_a a_{ij}^2 \tag{2.12}$$

Where III_a, II_a and I_a are invariants of the tensor a_{ij}. For now, the precise formulation of these invariants is unimportant. The power of a tensor is seen as a tensor product with itself, for example: $a_{ij}^2 = a_{ik}a_{kj}$. Any tensor group can now be reduced to one in which no tensor has a power greater than 2. This renders the number of tensor groups finite. More details may be found in (Durbin & Reif, 2010; Pope, 1975; Spencer & Rivlin, 1958). The 10 tensor groups in matrix notation are:

$$\begin{aligned}
&\mathbf{T^{(1)}} = \mathbf{S} && \mathbf{T^{(2)}} = \mathbf{S\Omega} - \mathbf{\Omega S}\\
&\mathbf{T^{(3)}} = \mathbf{S^2} - \frac{\mathbf{1}}{\mathbf{3}}\{\mathbf{S^2}\}\mathbf{I} && \mathbf{T^{(4)}} = \mathbf{\Omega^2} - \frac{\mathbf{1}}{\mathbf{3}}\{\mathbf{\Omega^2}\}\mathbf{I}\\
&\mathbf{T^{(5)}} = \mathbf{\Omega S^2} - \mathbf{S^2\Omega} && \mathbf{T^{(6)}} = \mathbf{\Omega^2 S} + \mathbf{S\Omega^2} - \frac{\mathbf{2}}{\mathbf{3}}\{\mathbf{S\Omega^2}\}\mathbf{I}\\
&\mathbf{T^{(7)}} = \mathbf{\Omega S\Omega^2} - \mathbf{\Omega^2 S\Omega} && \mathbf{T^{(8)}} = \mathbf{S\Omega S^2} - \mathbf{S^2\Omega S}\\
&\mathbf{T^{(9)}} = \mathbf{\Omega^2 S^2} + \mathbf{S^2\Omega^2} - \frac{\mathbf{2}}{\mathbf{3}}\{\mathbf{S^2\Omega^2}\}\mathbf{I} && \mathbf{T^{(10)}} = \mathbf{\Omega S^2\Omega^2} - \mathbf{\Omega^2 S^2\Omega}
\end{aligned} \tag{2.13}$$

Where $\mathbf{S}$ is a matrix representation of S_{ij}. A matrix raised to a power is a repeated matrix multiplication with itself, for example: $\mathbf{S}^2 = \mathbf{SS}$. Curly braces denote the trace operator, i.e. $\{\mathbf{S}\} = S_{ii}$. Note that the first tensor group is used in EVM, see Eq. 2.10. A non-linear relationship is thus a generalisation of which the Boussinesq hypothesis is a subset. EARSM/NLEVM use additional tensor groups in their relationship for a_{ij}. Their approach differs in the determination of the coefficients, α_n. NLEVM are in spirit similar to EVM, in that they calibrate the coefficients based on certain (basis) flows, either from experiments or high resolution computations. EARSM are formally derived from RSM, and thereby try to inherit certain characteristics of these models.

2.4. Explicit Algebraic Reynolds Stress Models

Explicit Algebraic Reynolds Stress Models are derived from the differential Reynolds Stress Models by invoking the weak equilibrium assumption to obtain an implicit expression for a_{ij}. These are solved to obtain an explicit expression for a_{ij}. An Explicit Algebraic Model can only strive to be as good as its underlying model. A short discussion of the differential equations and the weak equilibrium assumption provides insight in the capabilities of EARSM.

2.4.1. Differential Reynolds Stress Models

The differential Reynolds Stress Models are derived from the Navier Stokes equations. The mean flow equation, Eq. 2.2, is subtracted from the Navier-Stokes equations, resulting in equations for the velocity fluctuation u_i'. These equations are multiplied with u_j', resulting in the differential equations. For more details, see (Nieuwstadt et al., 2016; Pope, 2000). The resulting differential equations are:

$$\frac{D}{Dt}\overline{u_i'u_j'} + \frac{\partial}{\partial x_k}T_{kij} = \mathcal{P}_{ij} + \Pi_{ij} - \varepsilon_{ij} \tag{2.14}$$

With:

$$\text{Production}: \quad \mathcal{P}_{ij} = -\left(\overline{u_i'u_j'}\frac{\partial \overline{u}_j}{\partial x_k} + \overline{u_i'u_j'}\frac{\partial \overline{u}_i}{\partial x_k}\right) \tag{2.15}$$

$$\text{Transport}: \quad T_{kij} = \frac{1}{\rho}\overline{p'u_j'}\delta_{ik} + \frac{1}{\rho}\overline{p'u_i'}\delta_{jk} + \overline{u_i'u_j'u_k'} - \nu\frac{\partial \overline{u_i'u_j'}}{\partial x_k} \tag{2.16}$$

$$\text{Pressure-rate-of-strain}: \quad \Pi_{ij} = \overline{\frac{p'}{\rho}\left(\frac{\partial u_i'}{\partial x_j} + \frac{\partial u_j'}{\partial x_i}\right)} \tag{2.17}$$

$$\text{Dissipation}: \quad \varepsilon_{ij} = 2\nu\overline{\frac{\partial u_i'}{\partial x_k}\frac{\partial u_j'}{\partial x_k}} \tag{2.18}$$

In these models, the quantities $\overline{u_i'u_j'}$ and u_i' are part of the solution and can be regarded as 'known'. This differential equation is not closed and requires models for various terms. The production term is in closed form and doesn't require modelling. The transport term contains unknown correlations such as $\overline{p'u_i'}$ and $\overline{u_i'u_j'u_k'}$ which require modelling. This is, however, not important for EARSM. The weak equilibrium assumption, which is discussed later on, makes assumptions for this term so that a model is not required. The following term, the pressure-rate-of-strain tensor, again contains unknown correlations. It is the model for this term that also affects EARSM, as it inherits this model. Finally, the dissipation term does also require modelling. Usually, it is split in its isotropic and deviatoric part:

$$\varepsilon_{ij} = \frac{2}{3}\varepsilon\delta_{ij} + \tilde{\varepsilon}_{ij} \tag{2.19}$$

The effect of the anisotropic dissipation $\tilde{\varepsilon}_{ij}$ is generally taken in the model of the pressure-rate-of-strain tensor as they posses similar mathematical properties. The isotropic part ε is solved for via an additional transport equation. A detailed discussion on models for the pressure-rate-of-strain tensor is outside the scope of this thesis, however more details may be found in (Pope, 2000, Ch. 11).

Note that Eq. 2.14 may also be regarded as equations for the Reynolds stress anisotropy, as they are linked through Eq. 2.6. This motivates the use of the differential equation as a starting point for an algebraic expression for a_{ij}.

2.4.2. Weak Equilibrium Assumption

To obtain an algebraic expression from the differential equation, Eq. 2.14, two things are required: 1) the combined model for the pressure-rate-of-strain tensor and anisotropic dissipation needs to be an algebraic function of a_{ij}, S_{ij} and Ω_{ij}, i.e. $\Pi_{ij} + \tilde{\varepsilon}_{ij} = f(a_{ij}, S_{ij}, \Omega_{ij})$. This is generally satisfied by all pressure-rate-of-strain models. 2) The convection and transport terms, i.e. $\mathcal{D}_{ij} = \frac{D}{Dt}\overline{u_i'u_j'} + \frac{\partial}{\partial x_k}T_{kij}$, need to be approximated by an algebraic expression. The approximation used by EARSM is proposed by Rodi (1976), and is called the weak equilibrium assumption. The approximation of the convective

part is discussed by Pope (2000, Ch. 11) and the current explanation follows this. Note that the Reynolds stresses can be decomposed as:

$$\overline{u_i' u_j'} = k\frac{\overline{u_i' u_j'}}{k} = k\left(a_{ij} + \frac{2}{3}\delta_{ij}\right) \tag{2.20}$$

This illustrates that variations in Reynolds stresses are due to variations in a_{ij} and k. The weak equilibrium assumption can now be stated as: the variations in $\overline{u_i' u_j'}$ due to a_{ij} are neglected, however the variations due to k are retained. Using Eq. 2.20, the material derivative can be approximated as:

$$\frac{D}{Dt}\left(k\frac{\overline{u_i' u_j'}}{k}\right) = \frac{\overline{u_i' u_j'}}{k}\frac{Dk}{Dt} + k\frac{D}{Dt}\left(a_{ij} + \frac{2}{3}\delta_{ij}\right) \approx \frac{a_{ij}}{k}\frac{Dk}{Dt} \tag{2.21}$$

Equivalently, in literature the weak equilibrium assumption is also stated as:

$$\frac{Da_{ij}}{Dt} = 0 \tag{2.22}$$

For the approximation of the transport term, denote:

$$\mathcal{T}_{ij} = \frac{\partial}{\partial x_k} T_{kij} \tag{2.23}$$

Gatski and Jongen (2000) describe the approximation for the transport term $\mathcal{T}_{ij}$. In most cases, the following relationship is assumed:

$$\mathcal{T}_{ij} = \frac{\overline{u_i' u_j'}}{k}\frac{1}{2}\mathcal{T}_{kk} \tag{2.24}$$

Which effectively states that the anisotropy of the transport term is assumed proportional to the anisotropy of the Reynolds stresses. Gatski and Jongen (2000) also describe an alternative formulation for the transport term. This can be obtained by rewriting Eq. 2.24 in terms of Reynolds stress anisotropy:

$$\mathcal{T}_{ij} - \frac{\overline{u_i' u_j'}}{k}\frac{1}{2}\mathcal{T}_{kk} = \mathcal{T}_{ij} - \frac{a_{ij}}{2}\mathcal{T}_{kk} - \frac{1}{3}\delta_{ij}\mathcal{T}_{kk} = 0 \tag{2.25}$$

In this alternative formulation, the term proportional to a_{ij} is combined with a similar term that occurs in the pressure-rate-of-strain model. As opposed to Eq. 2.24, the deviatoric part of the transport term is then assumed to vanish:

$$\mathcal{T}_{ij} - \frac{1}{3}\delta_{ij}\mathcal{T}_{kk} = 0 \tag{2.26}$$

This alternative formulation is used by Carlson et al. (2001) for an improved computation of turbulent wakes. The two approximations for the transport term may be combined in a more general formulation, as reported by Gatski and Jongen (2000):

$$\mathcal{T}_{ij} - \frac{\overline{u_i' u_j'}}{k}\frac{1}{2}\mathcal{T}_{kk} = -\gamma\mathcal{T}_{kk}\frac{\overline{u_i' u_j'}}{2} \tag{2.27}$$

If $\gamma = 0$ then it amounts to Eq. 2.26, if $\gamma = 1$ then it is the same as Eq. 2.24. The approximations for the convection, Eq. 2.21, and transport terms, Eq. 2.27, can be combined to obtain an implicit algebraic expression for the Reynolds stresses. Combining Eq. 2.21 and Eq. 2.27:

$$\begin{aligned}
\frac{D}{Dt}\overline{u_i' u_j'} + \mathcal{T}_{ij} &= \frac{\overline{u_i' u_j'}}{k}\frac{Dk}{Dt} + \frac{\overline{u_i' u_j'}}{k}\frac{1}{2}\mathcal{T}_{kk} - \gamma\mathcal{T}_{kk}\frac{a_{ij}}{2} \\
&= \frac{\overline{u_i' u_j'}}{k}\left(\frac{Dk}{Dt} + \frac{\mathcal{T}_{kk}}{2}\right) - \gamma\mathcal{T}_{kk}\frac{a_{ij}}{2} \\
&= \frac{\overline{u_i' u_j'}}{k}\left(\mathcal{P}_{ij} - \varepsilon\right) - \gamma\mathcal{T}_{kk}\frac{a_{ij}}{2}
\end{aligned} \tag{2.28}$$

Where in the last step the balance for turbulent kinetic energy is used. This result may be substituted in Eq. 2.14, to obtain:

$$\frac{\overline{u_i' u_j'}}{k}\left(\mathcal{P}_{kk}-\varepsilon\right)-\gamma\mathcal{T}_{kk}\frac{a_{ij}}{2}=\mathcal{P}_{ij}+\left(\Pi_{ij}-\tilde{\varepsilon}_{ij}\right)-\frac{2}{3}\varepsilon\delta_{ij} \tag{2.29}$$

Using Eq. 2.6, it can be rewritten as

$$a_{ij}\left(\mathcal{P}_{kk}-\varepsilon-\gamma\frac{\mathcal{T}_{kk}}{2}\right)=\mathcal{P}_{ij}-\frac{2}{3}\delta_{ij}\mathcal{P}_{kk}+\left(\Pi_{ij}-\tilde{\varepsilon}_{ij}\right) \tag{2.30}$$

Combined with an algebraic model for the pressure-rate-of-strain correlations (Π_{ij}) and dissipation ($\tilde{\varepsilon}_{ij}$), it forms an (implicit) algebraic equation for a_{ij}.

2.4.3. Explicit Solution

The implicit equation Eq. 2.30, with an algebraic model for $\Pi_{ij}-\tilde{\varepsilon}_{ij}$, is the basis from which an explicit formulation is derived. It appears straight-forward to obtain an explicit solution for Eq. 2.30 if $\Pi_{ij}-\tilde{\varepsilon}_{ij}$ is linear in a_{ij}. It turns out, however, that Eq. 2.30 is nonlinear in the Reynolds stress anisotropy. This non-linearity enters through the turbulent kinetic energy production $\mathcal{P}_{kk}$, which is proportional to the trace of $\mathbf{aS}$. More specifically:

$$\mathcal{P}_{kk}=-a_{kl}S_{lk}\varepsilon \tag{2.31}$$

The Reynolds stress anisotropy enters the equation both via a trace and as a tensor. There is also another potential source for non-linearity, namely through the model of the pressure-rate-of-strain tensor. These models, similar to the Reynolds stress anisotropy, may be constructed as a linear combination of tensors. Pope (2000, Ch. 11) reports 8 tensor groups that have been used in RSM:

$$\begin{aligned}
\frac{\Pi_{ij}}{\varepsilon}&=\sum_i f^{(i)}\Gamma_{ij}^{(i)}\\
\mathbf{\Gamma^{(1)}}&=\mathbf{a}\\
\mathbf{\Gamma^{(2)}}&=\mathbf{a^2}-\frac{1}{3}\{\mathbf{a^2}\}\mathbf{I}\\
\mathbf{\Gamma^{(3)}}&=\mathbf{S}\\
\mathbf{\Gamma^{(4)}}&=\mathbf{Sa}+\mathbf{aS}-\frac{2}{3}\{\mathbf{Sa}\}\mathbf{I}\\
\mathbf{\Gamma^{(5)}}&=\mathbf{\Omega a}-\mathbf{a\Omega}\\
\mathbf{\Gamma^{(6)}}&=\mathbf{Sa^2}+\mathbf{a^2S}-\frac{2}{3}\{\mathbf{Sa^2}\}\mathbf{I}\\
\mathbf{\Gamma^{(7)}}&=\mathbf{\Omega a^2}-\mathbf{a^2\Omega}\\
\mathbf{\Gamma^{(8)}}&=\mathbf{aSa}-\frac{1}{3}\{\mathbf{Sa^2}\}\mathbf{I}
\end{aligned} \tag{2.32}$$

As may be seen, some groups are tensorally quadratic in the anisotropy ($\mathbf{\Gamma^{(2)}}, \mathbf{\Gamma^{(6)}}, \mathbf{\Gamma^{(7)}}, \mathbf{\Gamma^{(8)}}$). Generally, EARSM are limited to models whose tensor groups are linear in $\mathbf{a}$. This simplifies the algebra involved in obtaining an explicit solution. A general quasi-linear model would be (Hellsten & Wallin, 2009):

$$\begin{aligned}
\frac{\Pi_{ij}}{\varepsilon}=&-\frac{1}{2}\left(C_1^0+C_1^1\frac{\mathcal{P}_{kk}}{\varepsilon}\right)a_{ij}\\
&+C_2S_{ij}+\frac{C_3}{2}\left(a_{ik}S_{kj}+S_{ik}a_{kj}-\frac{2}{3}a_{kl}S_{lk}\delta_{ij}\right)\\
&-\frac{C_4}{2}\left(a_{ik}\Omega_{kj}-\Omega_{ik}a_{kj}\right)
\end{aligned} \tag{2.33}$$

As an additional complication, the coefficients in Eq. 2.33 may depend on invariants of a_{ij} and on $\mathcal{P}_{kk}/\varepsilon$. Pope (1975) was the first to solve this problem in an inertial frame in two dimensions. In his

approach, the full integrity basis Eq. 2.11 is substituted in Eq. 2.30 with Eq. 2.33. This essentially results in a linear system for the coefficients α_n:

$$\mathbf{A}\boldsymbol{\alpha} = \mathbf{b} \tag{2.34}$$

The coefficients may then be obtained by inversion of $\mathbf{A}$, which is by no means trivial. This is also why Pope only succeeded in 2D, where $\mathbf{A}$ is a 3x3 matrix. It is important to mention that $\mathcal{P}_{kk}/\varepsilon$ is still implicit in the solution, i.e. α_n still depends on $\mathcal{P}_{kk}/\varepsilon$ which in turn depends on a_{ij}. Gatski and Speziale (1993) found a solution in 3D for non-inertial frames based on the procedure by Pope (1975). The production-to-dissipation ratio $\mathcal{P}_{kk}/\varepsilon$ is still implicit in their solution. They circumvent this by using an asymptotic equilibrium value for $\mathcal{P}_{kk}/\varepsilon$, thus making it fully explicit. More recently, Wallin and Johansson (2000) proposed an EARSM using Pope's procedure for three dimensional flows in rotating frames. As opposed to Gatski and Speziale (1993), Pope (1975), they also derive and solve a non-linear scalar equation related to $\mathcal{P}_{kk}/\varepsilon$. Resulting in a fully explicit constitutive relationship for a_{ij}, without having to specify $\mathcal{P}_{kk}/\varepsilon$ *a priori*.

2.5. Non-Linear Eddy Viscosity Models

Non-Linear Eddy Viscosity Models (NLEVM) take a different approach than EARSM to deriving the coefficients in Eq. 2.11 and/or the constitutive relationship itself. This section describes some of these models. It is not meant as an exhaustive overview of models, instead the focus is on models with unique features that are different from EARSM. NLEVM are generally limited to quadratic or cubic groups in Eq. 2.13.

Apsley and Leschziner (1998) proposed a cubic model for a_{ij}. Instead of deriving the constitutive relationship directly using the procedure by Pope (1975), they proposed to use an iterative method. Eq. 2.30 is an implicit relationship that can be written as:

$$\mathbf{a} = \mathbf{b} + \mathbf{f}(\mathbf{a}) \tag{2.35}$$

Where $\mathbf{b}$ is a constant and equal to $c\mathbf{S}$, with some constant c, as a result of the pressure-rate-of-strain model in Eq. 2.33. Furthermore, $\mathbf{f}(\mathbf{a})$ is a tensor function, representing all terms on the right hand side of Eq. 2.30 that depend on $\mathbf{a}$. Successive approximations of $\mathbf{a}$ may then be obtained as:

$$\mathbf{a}^{(1)} = \mathbf{b}; \quad \mathbf{a}^{(n)} = \mathbf{b} + \mathbf{f}(\mathbf{a}^{(n-1)}) \quad \text{for } n = 2, 3, 4, ... \tag{2.36}$$

This procedure is mathematically simpler than solving the implicit expression directly. Furthermore, the model obtained this way cannot be singular, which may occur in EARSM. Apsley and Leschziner stopped at the third iteration, i.e. $n = 3$, to obtain a cubic model. In theory, the coefficients of this formulation depend on the underlying RSM. Apsley and Leschziner opted, however, to recalibrate their coefficients. In particular, because the underlying model was unsuitable in the near-wall region. With this recalibration, the model can be integrated through the boundary layer.

Abe et al. (2003) introduced a model to represent the correct stress anisotropies at the wall. This is an improvement on the work by Abe et al. (1997), which in turn is a low-Re modification of the model by Gatski and Speziale (1993). A novel feature in the model by Abe et al. (2003) is the introduction of a new tensor group $d_i d_j$. Here, d_i is a unit vector representing the wall normal direction, which they defined as:

$$d_i = \frac{N_i}{\sqrt{N_k N_k}}, \quad N_i = \frac{\partial l_d}{\partial x_i}, \quad l_d = n \tag{2.37}$$

Where n is the wall normal distance. Although Abe et al. (2003) note that alternative variables could be used. An example they provide is $l_d = k^{3/2}/\varepsilon$. This additional tensor group results in improved normal anisotropies in plane channel flow (Abe et al., 2003).

2.6. Validation for Separated Flows

Several studies are performed that compare the performance of EARSM/NLEVM with EVM, LES and/or experiments in separated flows (Apsley et al., 1997; Apsley & Leschziner, 2000; Franke et al., 2005; Jang et al., 2002; Lien & Leschziner, 1994; Wang et al., 2004). Similar conclusions were drawn in these studies. The (qualitative) prediction of non-linear models is generally better than linear eddy viscosity models, albeit not accurate per se. This improved accuracy is, however, not necessarily due to the non-linear tensors added by EARSM/NLEVM. Apsley and Leschziner (2000) found that the improvement is mainly due to the strain dependency in the eddy viscosity (related to α_1), for an asymmetric diffuser. The non-linear terms (and thus anisotropy) did improve the solution, but to a much lesser extent. This is supported by Lien and Leschziner (1994), who found little change in the solution due to the non-linear terms, in case of a backward facing step. Similarly, Apsley et al. (1997) noted that differences in models is mainly due to sensitivity of model coefficients to $\mathbf{S}$ and $\mathbf{\Omega}$, using a 'Aerospatial-A' airfoil as a test case.

These various studies observed similar behaviour of the separated flow in the wake. All models underpredict the turbulent kinetic energy in the separated region. This is found for 2D periodic hills (Apsley et al., 1997), a 3D hill (Wang et al., 2004) and the backward facing step (Lien & Leschziner, 1994). Associated with this, is an underprediction of the shear stress in the separated shear layer (Apsley et al., 1997; Jang et al., 2002; Lien & Leschziner, 1994). This amounts to reduced momentum transport in the cross-stream direction. Therefore, the momentum recovery in the wake is slower (Jang et al., 2002; Lien & Leschziner, 1994; Wang et al., 2004). As a result, longer and narrower recirculation zones are observed (Apsley et al., 1997; Jang et al., 2002; Wang et al., 2004). In addition, it has to be noted that the location of the reattachment point is strongly dependent on the precise location of separation (Apsley et al., 1997; Jang et al., 2002).

It is also noted by various authors that the accompanying turbulent transport equations may have a large effect (Abe et al., 2003; Franke et al., 2005; Jang et al., 2002). Models are observed to be sensitive to differences in functional form and coefficients (Apsley & Leschziner, 2000). Abe et al. (2003) validated his model with ω- and ε-based model, and noted that ω-based models may be advantageous for separated flow.

Lastly, an outlook to the rounded transom interceptor can be made. From a design perspective, it is interesting to know how separation affects the pressure distribution. Wang et al. (2004) reported the pressure distribution for a 3D hill. In addition, Franke et al. (2005) performed calculations for a ONERA-A airfoil and DLR F4 wing-body configuration. In all three cases it is found that the pressure is underpredicted in the separation zone.

2.7. Turbulence Model

This section presents the k-ω equations and associated EARSM that is implemented in this thesis.

2.7.1. Governing Equations

To reiterate, the governing RANS equations for incompressible flow are:

$$\frac{\partial \overline{u}_i}{\partial x_i} = 0 \tag{2.38}$$

$$\frac{\partial \overline{u}_i}{\partial t} + \overline{u}_j \frac{\partial \overline{u}_i}{\partial x_j} = \frac{1}{\rho}\frac{\partial \overline{p}}{\partial x_i} + \frac{\partial}{\partial x_j}\left(\nu\left(\frac{\partial \overline{u}_i}{\partial x_j} + \frac{\partial \overline{u}_j}{\partial x_i}\right)\right) - \frac{\partial \overline{u_i' u_j'}}{\partial x_j} + f_i \tag{2.39}$$

Where the Reynolds stress tensor $\overline{u_i' u_j'}$ in this thesis is defined as:

$$\overline{u_i' u_j'} = -\nu_T\left(\frac{\partial \overline{u}_i}{\partial x_j} + \frac{\partial \overline{u}_j}{\partial x_i}\right) + a_{ij}^{(ex)} k + \frac{2}{3} k \delta_{ij} \tag{2.40}$$

With ν_T being the eddy or turbulent, kinematic viscosity. The dimensionless, non-linear anisotropy are denoted by $a_{ij}^{(ex)}$. In the model by Hellsten (2005), the RANS equations are accompanied by two turbulent transport equations. Which are the turbulent kinetic energy k, and specific turbulent dissipation rate $\omega = \varepsilon / k$:

$$\frac{\partial k}{\partial t} + \overline{u}_j \frac{\partial k}{\partial x_j} = \mathcal{P} - \beta^* k\omega + \frac{\partial}{\partial x_j}\left((\nu + \sigma_k \nu_T)\frac{\partial k}{\partial x_j}\right) \tag{2.41}$$

$$\frac{\partial \omega}{\partial t} + \overline{u}_j \frac{\partial \omega}{\partial x_j} = \gamma \frac{\omega}{k}\mathcal{P} - \beta\omega^2 + \frac{\partial}{\partial x_j}\left((\nu + \sigma_\omega \nu_T)\frac{\partial \omega}{\partial x_j}\right) + \sigma_d \frac{1}{\omega}\max\left(\frac{\partial \omega}{\partial x_j}\frac{\partial k}{\partial x_j}, 0\right) \tag{2.42}$$

2.7.2. Zonal Coefficients

This model is conceptually similar to BSL / SST k-ω models of Menter, in that it is a zonal model. It switches between two sets of coefficients, near solid walls it operates as a k-ω model, far away it essentially becomes a k-ε model. This is accomplished by mixing the coefficients σ_k, σ_ω, σ_d, γ and β. These coefficients take the general form:

$$C = f_{\text{mix}} C_1 + (1 - f_{\text{mix}}) C_2 \tag{2.43}$$

The mixing function f_{mix} is a modified version of Menter's corresponding F_1 function, although based of similar ideas. The function approaches one near the edge of boundary layers, and is zero in free turbulent flows. It is defined as:

$$f_{\text{mix}} = \tanh(1.5\Gamma^4) \tag{2.44}$$

The parameter Γ is a function of three measures:

$$\Gamma = \min\left(\max\left(\Gamma_1, \Gamma_2\right), \Gamma_3\right) \tag{2.45}$$

With these measures being:

$$\Gamma_1 = \frac{\sqrt{k}}{\beta^* k\omega} \tag{2.46}$$

$$\Gamma_2 = \frac{500\nu}{\omega d^2} \tag{2.47}$$

$$\Gamma_3 = \frac{20k}{\max\left(d^2(\nabla k \cdot \nabla\omega)/\omega, 200k_\infty\right)} \tag{2.48}$$

The two sets of coefficients are:

Set	γ	β	σ_k	σ_ω	σ_d
1	0.518	0.0747	1.1	0.53	1.0
2	0.44	0.0828	1.1	1.0	0.4

2.7.3. Constitutive Model

Hellsten's proposed k-ω equations are designed to be used with Wallin & Johansson's constitutive relationship for the Reynolds stress tensor. The dimensionless anisotropy tensor (including both linear and non-linear terms) is defined as a tensor polynomial:

$$\begin{aligned} a_{ij} = {} & \beta_1 S_{ij} + \beta_3\left(\Omega_{ik}\Omega_{kj} - \frac{1}{3}II_\Omega\delta_{ij}\right) \\ & + \beta_4\left(S_{ij}\Omega_{kj} - \Omega_{ik}\Omega_{kj}\right) \\ & + \beta_6\left(S_{ik}\Omega_{kl}\Omega_{lj} + \Omega_{ik}\Omega_{kl}S_{lj} - \frac{2}{3}IV\delta_{ij}\right) \\ & + \beta_9\left(\Omega_{ik}S_{kl}\Omega_{lm}\Omega_{mj} - \Omega_{ik}\Omega_{kl}S_{lm}\Omega_{mj}\right) \end{aligned} \tag{2.49}$$

Which is a function of two dimensionless, kinematic tensors:

$$S_{ij} = \frac{\tau}{2}\left(\frac{\partial \overline{u}_i}{\partial x_j} + \frac{\partial \overline{u}_j}{\partial x_i}\right) \qquad \Omega_{ij} = \frac{\tau}{2}\left(\frac{\partial \overline{u}_i}{\partial x_j} - \frac{\partial \overline{u}_j}{\partial x_i}\right) \tag{2.50}$$

Where τ represents a time scale. Here, the formulation of Wallin & Johansson is used which include a viscous timescale as a lower limit. As noted by Hellsten, this may be dropped in a high Reynolds number formulation. For example, when law of the wall is used instead of resolving the boundary layer. The definition of the timescale is:

$$\tau = \max\left(\frac{1}{\beta^* \omega}, C_\tau \sqrt{\frac{\nu}{\beta^* k \omega}}\right) \tag{2.51}$$

The beta coefficients of the anisotropy formulation in Eq. 2.49 are functions of the invariants of the kinematic tensors of Eq. 2.50. Some of these invariants (II_Ω, IV) also appear in the anisotropy formulation. These invariants are:

$$\begin{aligned} II_S &= S_{kl} S_{lk} \\ II_\Omega &= \Omega_{kl} \Omega_{lk} \\ III_S &= S_{kl} S_{lm} S_{mk} \\ IV &= S_{kl} \Omega_{lm} \Omega_{mk} \end{aligned} \tag{2.52}$$

The beta coefficients itself are given by:

$$\begin{aligned} \beta_1 &= -N(2N^2 - 7II_\Omega)/Q \\ \beta_3 &= -12IV/(NQ) \\ \beta_4 &= -2(N^2 - 2II_\Omega)/Q \\ \beta_6 &= -6N/Q \\ \beta_9 &= 6/Q \end{aligned} \tag{2.53}$$

Where Q is:

$$Q = \frac{5}{6}\left(N^2 - 2II_\Omega\right)\left(2N^2 - II_\Omega\right) \tag{2.54}$$

And N:

$$N = \begin{cases} \frac{A'}{3} + (P_1 + \sqrt{P_2})^{\frac{1}{3}} + \text{sign}(P_1 - \sqrt{P_2})|P_1 - \sqrt{P_2}|^{\frac{1}{3}} & \text{for } P_2 \geq 0 \\ \frac{A'}{3} + 2(P_1^2 - P_2)^{\frac{1}{6}} \cos\left(\frac{1}{3}\arccos\left(P_1/\sqrt{P_1^2 - P2}\right)\right) & \text{for } P_2 < 0 \end{cases} \tag{2.55}$$

With:

$$P_1 = \left(\frac{A_3'^2}{27} + \frac{9}{20} II_S - \frac{2}{3} II_\Omega\right) A_3' \tag{2.56}$$

$$P_2 = P_1^2 - \left(\frac{A_3'^2}{9} + \frac{9}{10} II_S + \frac{2}{3} II_\Omega\right)^3 \tag{2.57}$$

And A_3' is defined as:

$$A_3' = \frac{9}{5} + \frac{9}{4} C_{\text{Diff}} \max\left(1 + \beta_1^{(eq)} II_S, 0\right) \tag{2.58}$$

The purpose of this term is to model diffusion of the anisotropy that is ignored in the weak equilibrium assumption. The parameter $\beta_1^{(eq)}$ is defined as:

$$\beta_1^{(eq)} = -\frac{6}{5}\left(\frac{N^{(eq)}}{N^{(eq)^2} - 2II_\Omega}\right) \tag{2.59}$$

And finally:

$$N^{(eq)} = \frac{81}{20} \qquad C_{\text{Diff}} = 2.2 \tag{2.60}$$

The anisotropy formulation is divided in a linear part, which is the eddy viscosity:

$$\nu_T = C_\mu k\tau \qquad C_\mu = -\frac{1}{2}(\beta_1 + II_\Omega \beta_6) \tag{2.61}$$

And a non-linear part, which is $a_{ij}^{(ex)}$:

$$\begin{aligned} a_{ij}^{(ex)} = &\beta_3 \left(\Omega_{ik}\Omega_{kj} - \frac{1}{3} II_\Omega \delta_{ij}\right) \\ &+ \beta_4 \left(S_{ik}\Omega_{kj} - \Omega_{ik}S_{kj}\right) \\ &+ \beta_6 \left(S_{ik}\Omega_{kl}\Omega_{lj} + \Omega_{ik}\Omega_{kl}S_{lj} - II_\Omega S_{ij} - \frac{2}{3} IV\delta_{ij}\right) \\ &+ \beta_9 \left(\Omega_{ik}S_{kl}\Omega_{lm}\Omega_{mj} - \Omega_{ik}\Omega_{kl}S_{lm}\Omega_{mj}\right) \end{aligned} \tag{2.62}$$

3

Finite Element Formulation

For partial differential equations to be solved by computers, they need to be transformed to a set of algebraic equations. This process is called discretization. One such discretization technique is Isogeometric Analysis (IGA), which is used in this thesis, and was first introduced by Hughes et al. (2005). IGA is a particular form of the Finite Element Method (FEM), which uses the same mathematical representation of geometries as in Computer Aided Design (CAD) programs. This technique allows for exact representation of geometries that are not possible in classical finite elements. This chapter provides a short introduction to the Finite Element Method, as it is the basis for IGA. First off, the approximation of the exact solution in FEM is introduced in section 1. Thereafter, section 2 presents the weighted residual technique. This forms the basis for obtaining algebraic equations from differential equations. Section 3 discusses the implementation of boundary conditions. Lastly, section 4 presents stabilisation techniques that are necessary for fluid flow.

3.1. Approximate Solution

The starting point for the Finite Element Method is a (set of) partial differential equation(s). For simplicity, consider the following scalar boundary value problem

$$\begin{aligned} \mathcal{L}(u) - f &= 0 \quad \text{on } \Omega \\ u &= g \quad \text{on } \Gamma_g \subset \Gamma \\ \nabla u \cdot \mathbf{n} &= h \quad \text{on } \Gamma_h \subset \Gamma \end{aligned} \tag{3.1}$$

Where u is the dependent variable and f a source term. The interioir domain is denoted by Ω with the boundary of the domain being Γ ($= \Gamma_g \cup \Gamma_h$). The boundary consists of two parts: one where a Dirichlet boundary condition is imposed (Γ_g) with a value g, and one where a Neumann condition is imposed (Γ_h) normal to the boundary with a value h. More complex boundary conditions are possible, however most boundary conditions of practical interest can be expressed as either Dirichlet or Neumann conditions. Lastly, $\mathcal{L}()$ is a linear differential operator. This may appear restrictive, especially since the Navier-Stokes equations are non-linear. In a numerical method, however, the Finite Element Method is applied to a linearised form, and an iterative method is used to solve the non-linear problem. The current discussion is therefore still useful for non-linear equations.

For most problems of engineering interest, there is no analytical solution to the boundary value problem. Approximations are thus needed to solve the problem. In FEM, the exact solution is approximated as a linear combination of predefined functions, which are called basis or shape functions

$$u \approx u^h = \sum_{j=1}^{N} a_j \phi_j \tag{3.2}$$

In a classical Finite Element Method the basis functions ϕ_j are usually linear functions. This is where IGA distinguishes itself from classical Finite Element Methods. IGA uses Non-Uniform Rational B-Splines (NURBS) as basis functions. These functions are also used in CAD programs to represent

geometries. Hughes et al. (2005) provides a short introduction to NURBS in the context of IGA, a more detailed description is given by Piegl and Tiller (1997) in the context of CAD programs. The coefficients a_j are called the degrees of freedom. In classical FEM, the degrees of freedom correspond to values of u^h at certain locations. This, however, is not the case in IGA. As will be shown later, this has consequences for the imposition of Dirichlet boundary conditions.

3.2. Weighted Residual Techniques

At this point, a formulation is required from which the degrees of freedom a_j can be determined. For now, assume that the boundary conditions are satisfied by the basis functions, so that only the interior domain needs to be considered. This will be revisited in the next section. It is useful to introduce the residual $R\left(u^h\right) = \mathcal{L}\left(u^h\right) - f$. Ideally, the residual is zero over the entire domain, as that means the exact solution is obtained. In general, however, this is not possible and the residual will be non zero. The idea is now to make the residual as small as possible. This is done by weighing the residual and requiring that the integral of the weighted residual is zero. For example, a weighing function that is unity over the entire domain can be interpreted as the residual being zero *on average* over the domain. Of course, different weighings can be used to minimise $R\left(u^h\right)$ in different ways.

Now, a single weighing function is not sufficient to uniquely determine N degrees of freedoms. This idea is therefore extended to N weighing functions

$$\int_\Omega \psi_j R\left(u^h\right) d\Omega = 0 \quad \text{for } j = 1 \ldots N \tag{3.3}$$

Where ψ_j is a weighing function (also called a test function). With $\mathcal{L}()$ being a linear operator ($Ldiffa_i\phi_i = a_i\mathcal{L}\left(\phi_i\right)$), this results in a linear algebraic system of equations.

$$\begin{aligned} \sum_{i=1}^{N} \int_\Omega \psi_j \left(\mathcal{L}\left(\phi_i\right) a_i - f\right) d\Omega = 0 \quad &\rightarrow \sum_{i=1}^{N} K_{ji} a_i = b_j \\ K_{ji} &= \int_\Omega \psi_j \mathcal{L}\left(\phi_i\right) d\Omega \\ b_j &= \int_\Omega \psi_j f d\Omega \end{aligned} \tag{3.4}$$

With 'suitable' choices for ψ_j and ϕ_i, this system may be solved by either a direct or iterative linear solver. To complete this system, a formulation for ψ_j is needed (with ϕ_i being a NURBS function in IGA). First off, Eq. 3.3 may be written more compactly by introducing a function w, such that

$$w = \sum_{j=1}^{N} \beta_j \psi_j \tag{3.5}$$

Where β_j are arbitrary coefficients, and usually taken as $\beta_j = 1$. The weighted residual approach can now be written as

$$\int_\Omega w R\left(u^h\right) d\Omega = 0 \tag{3.6}$$

Different choices of ψ_j will result in different methods. To illustrate this, three different possibilities for ψ_j will be mentioned.

3.2.1. Point Collocation

In this method, N points are selected at which is required that $R\left(u^h\right) = 0$. Conceptually, this is comparable to the Finite Difference Method, in that the differential equation is satisfied at a discrete set of points. Mathematically, this can be represented by the Dirac delta function $\psi_j = \delta(\mathbf{x} - \mathbf{x}_j)$. The weighted residual formulation is then

$$\int_\Omega \delta\left(\mathbf{x} - \mathbf{x}_j\right) R\left(u^h\right) d\Omega \quad \text{for } j = 1 \ldots N \tag{3.7}$$

3.2.2. Subdomain Collocation

In this case, the domain Ω is divided into N subdomains or cells (Ω_j). In each subdomain the integral of the residual is set to zero, so that the residual is zero *on average* within that subdomain. Conceptually, this is similar to the Finite Volume Method, in that both methods satisfy the integral equations in a local fashion. The corresponding test function for this approach is

$$\psi_j = \begin{cases} 1 \text{ if } \mathbf{x} \in \Omega_j \\ 0 \text{ if } \mathbf{x} \notin \Omega_j \end{cases} \tag{3.8}$$

3.2.3. Galerkin Method

For the Galerkin method, the test function is the same as the basis function, i.e. $\psi_j = \phi_j$. This is the starting point for many Finite Element Methods. The Galerkin method combined with certain differential equations (such as Poisson type equations) result in symmetric matrices (after integration by parts). Which is a favourable property to exploit for linear solvers. The weighted residual formulation becomes

$$\int_\Omega \phi_j R\left(u^h\right) d\Omega = 0 \text{ for } j = 1 \ldots N \tag{3.9}$$

3.3. Weak Formulations

The Finite Element Method does not use the Galerkin method of weighted residuals in the form given by Eq. 3.9 directly. It is combined with a process of integration by parts. This reduces or 'weakens' the continuity requirement for u^h. The various weak formulations introduced in the remainder of this chapter will be illustrated using the convection-diffusion equations. This equation serves as a model for the linearised Navier-Stokes and turbulent equations in this thesis. Consider the following convection-diffusion problem

$$\begin{aligned} \mathbf{a} \cdot \nabla u - \nabla \cdot (\kappa \nabla u) - f = 0 \quad & \text{on } \Omega \\ u = g \quad & \text{on } \Gamma_g \subset \Gamma \\ \kappa \nabla u \cdot \mathbf{n} = h \quad & \text{on } \Gamma_h \subset \Gamma \end{aligned} \tag{3.10}$$

Where $\mathbf{a}$ is the convection velocity and κ the diffusivity constant, and all other the same as in Eq. 3.1. The weighted residual formulation is then

$$\int_\Omega w\left(\mathbf{a} \cdot \nabla u^h - \nabla \cdot \left(\kappa \nabla u^h\right)\right) d\Omega = 0 \tag{3.11}$$

3.3.1. Traditional Formulation

In the usual presentation of the Finite Element Method, this formulation is followed by a single integration by parts. This presents a choice for the convective term. It can either be integrated by parts or not. Either way, it does not affect the continuity requirement for u^h. In this thesis, only the diffusion term is integrated by parts. The resulting weak formulation is

$$\int_\Omega \kappa \nabla w \nabla u^h d\Omega + \int_\Omega w\left(\mathbf{a} \cdot \nabla u^h\right) d\Omega - \int_\Gamma w\left(\kappa \nabla u^h \cdot \mathbf{n}\right) d\Gamma = \int_\Omega w f d\Omega \tag{3.12}$$

The boundary integral term can be split into two parts, i.e. Γ_g and Γ_h. Applying the Neumann boundary condition, this results in

$$\int_\Omega \kappa \nabla w \nabla u^h d\Omega + \int_\Omega w\left(\mathbf{a} \cdot \nabla u^h\right) d\Omega - \int_{\Gamma_g} w\left(\kappa \nabla u \cdot \mathbf{n}\right) d\Gamma = \int_{\Gamma_h} w h d\Gamma + \int_\Omega w f d\Omega \tag{3.13}$$

Usually, Finite Element Methods require that Dirichlet boundary conditions are satisfied by the approximation. I.e., a subset of the degrees of freedoms are fixed such that $u^h = g$ on Γ_g. A homogeneous boundary condition is then imposed on the test function w, i.e. $w = 0$ on Γ_g. As a result, the third term in Eq. 3.13 disappears. Thus the weak form becomes

$$\int_\Omega \kappa \nabla w \nabla u^h d\Omega + \int_\Omega w\left(\mathbf{a} \cdot \nabla u^h\right) d\Omega = \int_{\Gamma_h} w h d\Gamma + \int_\Omega w f d\Omega \tag{3.14}$$

3.3.2. Residual Formulation

There is a more illuminating approach to obtain the weak formulation, which provides insight into the role of boundary conditions in FEM. The starting point is again the weighted residual formulation in Eq. 3.11. First, the diffusion term is integrated by parts. Thereafter, both the convection and diffusion terms are integrated by parts. This has the effect that the differential operators on Ω are 'transferred' from u^h to w, resulting in the adjoint operator

$$\begin{aligned} &\int_\Omega u^h \left(-\nabla\cdot(\kappa\nabla w) - \mathbf{a}\cdot\nabla w - f\right) d\Omega \\ &- \int_\Gamma w\left(\kappa\nabla u^h\cdot\mathbf{n}\right) d\Gamma \\ &+ \int_\Gamma u^h\left(\kappa\nabla w + \mathbf{a}w\right)\cdot\mathbf{n} d\Gamma = 0 \end{aligned} \tag{3.15}$$

Now, the integrals on the boundary Γ are split to obtain integrals on both Γ_g and Γ_h. Substituting the boundary conditions results In

$$\begin{aligned} &\int_\Omega u^h \left(-\nabla\cdot(\kappa\nabla w) - \mathbf{a}\cdot\nabla w - f\right) d\Omega \\ &- \int_{\Gamma_g} w\left(\kappa\nabla u^h\cdot\mathbf{n}\right) d\Gamma \\ &+ \int_{\Gamma_g} g\left(\kappa\nabla w + \mathbf{a}w\right)\cdot\mathbf{n} d\Gamma + \int_{\Gamma_h} u^h\left(\kappa\nabla w + \mathbf{a}w\right)\cdot\mathbf{n} d\Gamma \end{aligned} \tag{3.16}$$

To obtain the residual formulation, integration by parts is applied again. As before, first the diffusion term and thereafter both the diffusion and convection terms. As a result, the differential operators are 'transferred' back to u^h. The resulting formulation becomes

$$\begin{aligned} &\int_\Omega w\left(\mathbf{a}\cdot\nabla u^h - \nabla\cdot(\kappa\nabla u^h) - f\right)\, d\Omega \\ &- \int_{\Gamma_1} w\ \kappa\nabla u^h\cdot\mathbf{n}\, d\Gamma - \int_{\Gamma_2} w\overline{q}\, d\Gamma + \int_\Gamma w\ \kappa\nabla u^h\cdot\mathbf{n}\, d\Gamma \\ &+ \int_{\Gamma_1} (\kappa\nabla w + \mathbf{a}w)\cdot\mathbf{n}\ \overline{u}\, d\Gamma + \int_{\Gamma_2} (\kappa\nabla w + \mathbf{a}w)\cdot\mathbf{n}\ u^h\, d\Gamma - \int_\Gamma (\kappa\nabla w + \mathbf{a}w)\cdot\mathbf{n}\ u^h\, d\Gamma = 0 \end{aligned} \tag{3.17}$$

The residual formulation is obtained by splitting the boundary integral into its sub-boundaries (Γ_1 & Γ_2) and simplyfing the expression

$$\begin{aligned} &\int_\Omega w\left(\mathbf{a}\cdot\nabla u^h - \nabla\cdot(\kappa\nabla u^h) - f\right)\, d\Omega \\ &+ \int_{\Gamma_2} w\ \left(\kappa\nabla u^h\cdot\mathbf{n} - \overline{q}\right)\, d\Gamma \\ &- \int_{\Gamma_1} (\kappa\nabla w + \mathbf{a}w)\cdot\mathbf{n}\ \left(u^h - \overline{u}\right)\, d\Gamma = 0 \end{aligned} \tag{3.18}$$

Notice that the result contains the residual on the interior ($R = \mathbf{a}\cdot\nabla u^h - \nabla\cdot(\kappa\nabla u^h) - f$), a residual for the Dirichlet condition ($R_1 = u^h - \overline{u}$) and a residual for the Neumann condition ($R_2 = \kappa\nabla u^h\cdot\mathbf{n} - \overline{q}$). So, this is the weighted residual formulation incorperating the effect of boundary conditions. This formulation may serve as a starting point for methods that do not enforce boundary conditions in the approximation of u^h. The weak formulation is obtained by integrating the diffusion term by parts

$$\begin{aligned} &\int_\Omega \kappa\nabla w\nabla u^h\, d\Omega + \int_\Omega w\left(\mathbf{a}\cdot\nabla u^h - f\right)\, d\Omega - \int_{\Gamma_2} \overline{q}\, d\Gamma \\ &- \int_{\Gamma_1} w\ \left(\kappa\nabla u^h\cdot\mathbf{n}\right)\, d\Gamma - \int_{\Gamma_1} (\kappa\nabla w + \mathbf{a}w)\cdot\mathbf{n}\ \left(u^h - \overline{u}\right)\, d\Gamma = 0 \end{aligned} \tag{3.19}$$

If the Dirichlet condition is satisfied by the approximation, i.e. $u^h = \overline{u}$, so that the residual R_1 is identically zero with $w = 0$ on Γ_1, then the traditional formulation is retrieved.

3.4. Stabilisation Techniques

The Galerkin weak formulation, $w = \sum \beta_j \psi_j = \sum \beta_j \phi_j$, is not suitable for flow problems. It suffers from two problems. First, spurious oscillations occur in convection dominated flows. Secondly, for incompressible flows, the pressure and velocity components cannot be represented by the same basis functions. These problems may be overcome by "stabilising" the formulation. Effectively, this means that the weighing function w is modified in some way, resulting in Petrov-Galerkin formulations. This section presents various stabilisation techniques that solve either or both deficiencies of the Galerkin formulation.

3.4.1. Streamline-Upwind / Petrov-Galerkin

A popular stabilisation technique for convection dominated problems is the Streamline-Upwind / Petrov-Galerkin (SUPG) method, introduced by Brooks and Hughes (1982). It aims to remedy spurious oscillations that may occur in convection dominated flows. SUPG achieves this in a manner similar to upwinding in Finite Volume Methods, in that it adds diffusivity in the stream-wise direction. Earlier methods also followed this approach, however they suffered from too much diffusion in the cross-stream direction (See Brooks & Hughes, 1982). The core of the SUPG method is the addition of an weak, anisotropic diffusion term

$$\int_\Omega (\mathbf{a} \cdot \nabla w)(\mathbf{a} \cdot \nabla u^h)\, d\Omega \tag{3.20}$$

This term can interpreted as a diffusion term in which the diffusivity constant κ is now a tensor $\kappa_{ij} = a_i a_j$. This tensor is the outer product of convection vector, and acts thus in the direction of convection. By itself, this term results in an inconsistent formulation. Meaning that the integral is non-zero for the exact solution, for which the residual R is zero. Therefore, Eq. 3.20 is modified to apply for the entire residual, so that the weighted residual becomes

$$\begin{aligned} &\int_\Omega wR\, d\Omega + \int_\Omega \mathbf{a} \cdot \nabla w R\, d\Omega = \\ &\int_\Omega (w + \mathbf{a} \cdot \nabla w) R\, d\Omega = 0 \end{aligned} \tag{3.21}$$

One can regard this formulation also as a modified Galerkin method ($\psi_j = \phi_j$). This class of modified Galerkin methods are also called Petrov-Galerkin methods. For the SUPG method, the test function ψ_j in Eq. 3.3 can be written as

$$\psi_j = \phi_j + \mathbf{a} \cdot \nabla \phi_j \tag{3.22}$$

3.4.2. Pressure-Stabilised / Petrov-Galerkin

Another scenario in which spurious oscillations might occur, is in mixed problems. For example, the Stokes and incompressible Navier-Stokes equations. In these equations, oscillations might occur in the pressure field when the same shape function is used for both velocity and pressure. The Pressure-Stabilised/Petrov-Galerkin (PSPG) aims to rectify this. This method is best described by illustration. Consider the Stokes equations

$$\begin{aligned} \nabla p - \nu \nabla^2 \mathbf{u} &= \mathbf{f} \\ \nabla \cdot \mathbf{u} &= 0 \end{aligned} \tag{3.23}$$

Which is a mixed problem for the velocity $\mathbf{u}$ and pressure p. With $\mathbf{f}$ a source term and ν kinematic viscosity. It may be written as

$$\begin{aligned} \mathcal{L}(\mathbf{u}, p) - \mathbf{f} &= 0 \\ \mathcal{L}(\mathbf{u}, p) = \begin{bmatrix} \nabla p - \nu \nabla^2 \mathbf{u} \\ \nabla \cdot \mathbf{u} \end{bmatrix} \qquad \mathbf{f} &= \begin{bmatrix} f \\ 0 \end{bmatrix} \end{aligned} \tag{3.24}$$

Where the weighted residual formulation is obtained by taking the dot product with a vector of shape functions $\mathbf{v}$. In general, different test function may be defined for the momentum & continuity equation, so that

$$\mathbf{v} = \begin{bmatrix} \mathbf{w} \\ q \end{bmatrix} \quad w_i = \sum_{j=1}^{N} \beta_{i,j}\psi_j \quad q = \sum_{j=1}^{N} \alpha_j \varphi_j \tag{3.25}$$

Where $\mathbf{w}$ is a vector of test functions, one for each momentum equation, and q is the test function for the continuity equation. Furthermore, ψ_j and φ_j are functions from the space of test functions and $\beta_{i,j}$ and α_j are arbitrary coefficients. The weighted residual formulation is then

$$\begin{aligned} &\int_\Omega \mathbf{v} \cdot (\mathcal{L}(\mathbf{u}, p) - \mathbf{f})\, d\Omega = \\ &\int_\Omega \mathbf{w} \cdot (\nabla p - \nu \nabla^2 \mathbf{u} - \mathbf{f})\, d\Omega + \int_\Omega q \nabla \cdot \mathbf{u}\, d\Omega = 0 \end{aligned} \tag{3.26}$$

Which is a more compact way of writing a set of $4N$ (in 3D), or $3N$ (in 2D), equations, similar to Eq. 3.3

$$\int_\Omega \psi_j (\nabla p - \nu \nabla^2 u_i - f_i)\, d\Omega \text{ for } j = 1 \ldots N \tag{3.27}$$

$$\int_\Omega \varphi_j \nabla \cdot \mathbf{u}\, d\Omega \text{ for } j = 1 \ldots N \tag{3.28}$$

The PSPG method is then given by the addition of (See Fries & Matthies, 2004)

$$\int_\Omega \tau \nabla q \cdot (\nabla p - \nu \nabla^2 \mathbf{u} - \mathbf{f})\, d\Omega \tag{3.29}$$

to the weighted residual formulation. Where τ is a suitable stabilisation parameter, which may be different than the one used in SUPG. The most important effect of PSPG is the addition of a pressure diffusion like term to Eq. 3.28. The PSPG method may then be summarised as

$$\int_\Omega \mathbf{w} \cdot (\nabla p - \nu \nabla^2 \mathbf{u} - \mathbf{f})\, d\Omega + \int_\Omega q \nabla \cdot \mathbf{u}\, d\Omega + \int_\Omega \tau \nabla q \cdot (\nabla p - \nu \nabla^2 \mathbf{u} - \mathbf{f}) = 0 \tag{3.30}$$

3.4.3. Galerkin Least Squares

There is a more general stabilisation technique that encompasses the effects of both SUPG and PSPG. This is the Galerkin / Least-Squares (GLS) method, introduced by Hughes et al. (1989). It achieves this by adding a least-squares term of the residual to the Galerkin formulation. A benefit of this approach over SUPG / PSPG is that it can be systematically applied to a wide variety of problems. To illustrate the least-squares term, consider again a linear scalar problem

$$\mathcal{L}(u^h) - f = 0 \tag{3.31}$$

In a least squares method, one wishes to minimise the square of the residual over the domain. This results in some sort of an objective function to minimise

$$I = \frac{1}{2} \int_\Omega \left(\mathcal{L}(u^h) - f\right)^2 d\Omega = \frac{1}{2} \int_\Omega \left(\sum_{j=1}^{N} \mathcal{L}(\phi_i) a_i - f \right)^2 d\Omega \tag{3.32}$$

Where a factor of one half is added for convience, and will cancel later on. The minimum of this function is retrieved when the partial dirivative of I with respect to every degree of freedom is zero

$$\frac{dI}{da_j} = \int_\Omega \mathcal{L}(\phi_j) \left(\sum_{i=1}^{N} \mathcal{L}(\phi_i) a_i - f \right) d\Omega = 0 \text{ for } j = 1 \ldots N \tag{3.33}$$

Note the presence of the residual $R = \sum_i^N \mathcal{L}(\phi_i)a_i - f$, so that this can also be regarded as a weighted residual formulation. The weighing function is then $\psi_j = \mathcal{L}(\phi_j)$. As the weighing functions are based on the same functions used for the approximation of u^h, this is a (Petrov-)Galerkin method. The addition of Eq. 3.33 to the Galerkin formulation completes the GLS method. It can then be summarised as

$$\int_\Omega (w + \tau\mathcal{L}(w))(\mathcal{L}(u^h) - f)\ d\Omega = 0 \tag{3.34}$$

Where τ is a stabilisation parameter. Or written as a set of weighted residuals

$$\begin{gathered}\sum_{i=1}^{N} \int_\Omega (\phi_j + \tau\mathcal{L}(\phi_j))(\mathcal{L}(\phi_i a_i) - f)\ d\Omega = 0 \text{ for } j = 1 \dots N \\ \psi_j = \phi_j + \tau\mathcal{L}(\phi_j)\end{gathered} \tag{3.35}$$

3.4.4. Variational Multiscale

Lastly, another stabilisation technique is Variational Multiscale (VMS). It is based on the notion that the Galerkin method is unsuitable for problems exhibiting multiscale phenomena. Fluid flow is an obvious example of multiscale phenomena. For convience, another way of writing integrals is introduced

$$(u, v)_\Omega = \int_\Omega uv\ d\Omega \tag{3.36}$$

The starting point of the Variational Multiscale method is to split the test function and solution in two scales

$$u = \overline{u} + u' \quad w = \overline{w} + w' \tag{3.37}$$

In the context of stabilised methods, $\overline{u} = u^h$ & $\overline{w} = w^h$ (i.e. the numerical approximation) are the resolved scales and u' & w' are the unresolved scales. The weighted residual formulation is then

$$\begin{gathered}(\overline{w} + w', \mathcal{L}(\overline{u} + u') - f)_\Omega = \\ (\overline{w}, \mathcal{L}(\overline{u} + u') - f)_\Omega + (w', \mathcal{L}(\overline{u} + u') - f)_\Omega = \\ (\overline{w}, \mathcal{L}(\overline{u}) - f)_\Omega + (\overline{w}, \mathcal{L}(u'))_\Omega + (w', \mathcal{L}(u'))_\Omega + (w', \mathcal{L}(\overline{u}) - f)_\Omega = 0\end{gathered} \tag{3.38}$$

Due to the fact that $\overline{w}$ and w' are linearly independent, they can be split into two problems

$$(\overline{w}, \mathcal{L}(\overline{u}) - f)_\Omega + (\overline{w}, \mathcal{L}(u'))_\Omega = 0 \tag{3.39}$$
$$(w', \mathcal{L}(\overline{u}) - f)_\Omega + (w', \mathcal{L}(u'))_\Omega = 0 \tag{3.40}$$

At this point, integration by parts is applied to the second integral of Eq. 3.39, so that the differential operators "shift" to $\overline{w}$. As a result, the adjoint operator $\mathcal{L}^*$ appears

$$(\overline{w}, \mathcal{L}(\overline{u}) - f)_\Omega + (\mathcal{L}^*(\overline{w}), u')_\Omega = 0 \tag{3.41}$$
$$(w', \mathcal{L}(\overline{u}) - f)_\Omega + (w', \mathcal{L}(u'))_\Omega = 0 \tag{3.42}$$

There are two important observations to be made from these equations. First, the resolved scales equations requires a formulation for u'. This formulation will be an approximation, as otherwise it results in the exact solution. Secondly, the unresolved scales are driven by the residual of the resolved scales. A stabilised formulation is obtained by approximating u' as

$$u' \approx -\tau(\mathcal{L}(u^h) - f) \tag{3.43}$$

With τ, again, being a stabilisation parameter. The stabilised weak formulation is then

$$\int_\Omega w^h(\mathcal{L}(u^h) - f)\ d\Omega - \int_\Omega \mathcal{L}^*(w^h)\tau(\mathcal{L}(u^h) - f)\ d\Omega = 0 \tag{3.44}$$

Or as a set of weighted residuals

$$\int_\Omega (\phi_j - \tau \mathcal{L}^* \phi_j)(\mathcal{L}u^h - f)\, d\Omega = 0 \text{ for } j = 1 \ldots N$$
$$\psi_j = \phi_j - \tau \mathcal{L}^* \phi_j \tag{3.45}$$

3.4.5. Stabilised System of Equations

The stabilisation methods introduced so far used a stabilisation parameter τ. It is, however, noted by Hughes and Mallet (1986) that a single parameter cannot simultaneously control all equations optimally. Only one component will behave optimally at most, while the others are overly diffusive. They proposed to use a stabilisation matrix $\boldsymbol{\tau}$. Hughes and Mallet (1986) considered a system of convection-diffusion equations with the SUPG method. Their approach can also be extended to different equations. The general approach is to diagonalize the system of equations and derive stabilisation parameters, for the now decoupled, components. This results in a diagonal stabilisation matrix, which is transformed back to use in the original formulation. As a starting point, consider a linear system of equations:

$$\frac{\partial \mathbf{U}}{\partial t} + \mathbf{A}_j \frac{\partial \mathbf{U}}{\partial x_j} = \frac{\partial}{\partial x_i}\left(\mathbf{K}_{ij} \frac{\partial \mathbf{U}}{\partial x_j}\right) + \mathbf{F} \tag{3.46}$$

Where $\mathbf{U}$ is the solution vector, $\mathbf{A}_j$ is the convection matrix, $\mathbf{K}_{ij}$ represents diffusivity and lastly $\mathbf{F}$ are source terms. In a lot of physical processes, $\mathbf{K}_{ij}$ is a diagonal matrix. This means that the system can be diagonalized via an eigenvalue decomposition of $\mathbf{A}_j$. It is important to emphasise that $\mathbf{A}_j$ are multiple matrices, one for each direction. It is assumed that we can diagonalize all $\mathbf{A}_j$ with the same transformation matrix. The weak formulation is:

$$\begin{aligned} &\int \mathbf{v} \cdot \left(\frac{\partial \mathbf{U}}{\partial t} + \mathbf{A}_j \frac{\partial}{\partial x_j}\mathbf{U} - \mathbf{F}\right) + \frac{\partial}{\partial x_j}\mathbf{v} \cdot \left(\mathbf{K}_j \frac{\partial}{\partial x_j}\mathbf{U}\right) \\ &+ \int \mathbf{d} \cdot \left(\frac{\partial}{\partial t}\mathbf{U} + \mathbf{A}_j \frac{\partial}{\partial x_j}\mathbf{U} - \frac{\partial}{\partial x_i}\left(\mathbf{K}_{ij}\frac{\partial}{\partial x_j}\mathbf{U}\right) - \mathbf{F}\right) = 0 \end{aligned} \tag{3.47}$$

Where Hughes and Mallet (1986) proposed for multi-dimensional systems:

$$\mathbf{d} = \boldsymbol{\tau}\left(\mathbf{A}_j \frac{\partial}{\partial x_j}\mathbf{v}\right) \tag{3.48}$$

Which is SUPG in multiple dimensions. The following transformation of variables is used to decouple the components:

$$\mathbf{U} = \mathbf{P}\mathbf{X} \qquad \mathbf{v} = \mathbf{P}\mathbf{Z} \tag{3.49}$$

Where $\mathbf{P}$ is a matrix whose columns are the eigenvectors of (all) $\mathbf{A}_j$. Furthermore, $\mathbf{D}$ is diagonal matrix with the eigenvalues of $\mathbf{A}_j$. In general, the eigenvalue decomposition of $\mathbf{A}_j$ is:

$$\mathbf{A}_j = \mathbf{P}\mathbf{D}\mathbf{P}^{-1} \tag{3.50}$$

if and only if $\mathbf{A}_j$ is a symmetric matrix, then it is orthogonally diagonalizable, so that:

$$\mathbf{A}_j = \mathbf{P}\mathbf{D}\mathbf{P}^T \tag{3.51}$$

Hughes and Mallet (1986) derived their results for a system in a symmetric form, i.e. $\mathbf{A}_j$ is symmetric. A symmetric form of the linearised incompressible Navier-Stokes exists (Franca & Hughes, 1993). Eq. 3.46 may then be thought of as the linearised Navier-Stokes equation. Using Eq. 3.51, a decoupled system is then obtained:

$$\begin{aligned} &\int \mathbf{Z} \cdot \left(\frac{\partial}{\partial t}\mathbf{X} + \mathbf{D}_j \frac{\partial}{\partial x_j}\mathbf{X} - \mathbf{P}^T\mathbf{F}\right) + \frac{\partial}{\partial x_i}\mathbf{Z} \cdot \left(\mathbf{P}^T\mathbf{K}_j\mathbf{P}\frac{\partial}{\partial x_j}\mathbf{X}\right) \\ &+ \left(\hat{\boldsymbol{\tau}}\mathbf{D}_j \frac{\partial}{\partial x_j}\mathbf{Z}\right) \cdot \left(\frac{\partial}{\partial t}\mathbf{X} + \mathbf{D}_j \frac{\partial}{\partial x_j}\mathbf{X} - \frac{\partial}{\partial x_i}\left(\mathbf{P}^T\mathbf{K}_{ij}\mathbf{P}\frac{\partial}{\partial x_j}\mathbf{X}\right) - \mathbf{P}^T\mathbf{F}\right) = 0 \end{aligned} \tag{3.52}$$

Which is indeed decoupled if the diffusivity matrices $\mathbf{K}_j$ are diagonal, and the assumptions on $\mathbf{A}_j$ hold. The diagonal stabilisation matrix $\hat{\tau}$ is defined as:

$$\boldsymbol{\tau} = \mathbf{P}\hat{\boldsymbol{\tau}}\mathbf{P}^T \tag{3.53}$$

Hughes and Mallet (1986) proposed a formulation for $\boldsymbol{\tau}$ for a convection-dominated case in which $\mathbf{A}_j$ are cast in a symmetric form. Consider a master element in a space with coordinates ε. Assume there is a mapping from this master space to the physical space $\mathbf{x} = \mathbf{x}(\varepsilon)$ and an inverse mapping $\varepsilon = \varepsilon(\mathbf{x})$. For example, a unit cube would be a master element which can be mapped to a parallelopiped in physical space. The convection matrix $\mathbf{A}_j$ can then be mapped to this master space:

$$\mathbf{B}_i = \left(\frac{\partial \varepsilon_i}{\partial x_j}\mathbf{A}_j\right) \tag{3.54}$$

Where $\mathbf{B}_i$ are the convection matrices in master space. Hughes and Mallet (1986) then defined $\boldsymbol{\tau}$, for square $\mathbf{B}_i$, as:

$$\boldsymbol{\tau} = \left(\left(\sum \left|\hat{\mathbf{B}}_i\right|^p\right)^{1/p}\right)^{-1} \tag{3.55}$$

3.5. Discontinuity Capture

The stabilisation methods discussed so far prevent oscillations in either the velocity or pressure field (or both in case of GLS). However, over- and undershoots may still occur is regions with large gradients, such as in boundary layers. Hughes et al. (1986) proposed a method similar to SUPG to capture discontinuities. It applies stabilisation in direction of $\nabla\phi$, in a way that SUPG applies stabilisation in direction of convection. The additional stabilisation term is

$$\int_\Omega \tau_{DC}(\mathbf{a}_\parallel \cdot \nabla w)(\mathbf{a}_\parallel \cdot \nabla u^h)\, d\Omega \tag{3.56}$$

Where τ_{DC} is again a stabilisation parameter and $\mathbf{a}_\parallel$ is the velocity projected in the direction of ∇u^h. It is defined as

$$\mathbf{a}_\parallel = \begin{cases} \dfrac{\mathbf{a}\cdot\nabla u^h}{|\nabla u^h|_2^2}\nabla u^h & \text{if } \nabla u^h \neq 0 \\ 0 & \text{if } \nabla u^h = 0 \end{cases} \tag{3.57}$$

3.6. Boundary Conditions

s Two types of boundary conditions are generally distinguished in finite element literature. 1) Those that occur in the weak formulation due to integration by parts, called natural boundary conditions and 2) those that are set explicitly in ϕ^h, called essential boundary conditions. Natural boundary conditions are of the Neumann-type, whereas essential boundary conditions are of the Dirichlet-type. This way of prescribing Dirichlet boundary conditions, through the definition of ϕ^h, is also referred to as a strong Dirichlet boundary condition. There is, however, another way to impose Dirichlet boundary conditions by introducing additional terms in the weak formulation. This approach is called a weak Dirichlet boundary condition. Bazilevs and Hughes (2007) compared weak Dirichlet to strong Dirichlet boundary conditions. In their work, they essentially introduce 2 to 3 terms to enforce Dirichlet boundary conditions. The most important one is a penalty like term:

$$\sum_b^{n_{eb}} \left(\mathbf{w}\frac{C_b\kappa}{h_b}, \mathbf{u} - \mathbf{g}\right)_\Omega \tag{3.58}$$

Where C_b is a constant, κ is diffusivity, h_b is the element size, $\mathbf{u}$ a vector of solution variables and $\mathbf{g}$ a vector of prescribed values. It works like a reaction term, whose strength is dependent on the mismatch with the prescribed value. Secondly, additional terms may be applied to the in- and outflow boundaries. If 2 terms are introduced, these are the same and of the form:

$$\sum_{b}^{n_{eb}} (\kappa \nabla \mathbf{w} \cdot \mathbf{n}, \mathbf{u} - \mathbf{g})_{\Omega} \tag{3.59}$$

The inflow boundary condition weighing function may be enhanced with a convective part so that more weight is put on the inflow than the outflow. Bazilevs and Hughes (2007) found improved convergence behaviour for unresolved boundary layers in channel flow. They noticed that the weak boundary condition behaved similarly to wall functions, even though they weren't designed as such.

This observation was explored further by Bazilevs et al. (2007), who designed the penalty term based on the law of the wall. They found improved performance with respect to the original weak Dirichlet formulation. Furthermore, Bazilevs et al. (2007) found that their new formulation reduced to a strong-like formulation with sufficient refinement in the wall normal direction. Indicating that this formulation may be suitable as a general no-slip boundary conditions in industrial applications.

4

Numerical Implementation

The Reynolds averaged Navier-Stokes equations and the accompanying turbulent equations are a difficult set of equations to solve numerically. The finite element formulation of the turbulent equations will generally not result in a robust method. This chapter describes the numerical implementation of these equations. The first and second section deals with modifications to the set of equations for improved robustness. The third and fourth section details a solution procedure for the coupled, non-linear equations.

4.1. Realizability of Turbulence Quantities

One source of difficulty in the RANS equations, is that they are subject to realizability constraints. This means that the results should be physically attainable. These constraints are not necessarily satisfied by the discretised equations and/or turbulence model. The realizability constraints for the Reynolds stresses

$$\overline{u_i'^2} \geq 0 \tag{4.1}$$

$$\left(\overline{u_i' u_j'}\right)^2 \leq \overline{u_i'^2}\ \overline{u_j'^2} \tag{4.2}$$

are generally not satisfied. Note that there is no summation implied in Eq. 4.1 and 4.2. Not satisfying the realizability constraints is sometimes by design, as to improve performance for flows of engineering interest. This generally does not result in numerical problems. On the other hand, the turbulent quantities used in this thesis come with their own realizability conditions

$$k \geq 0 \tag{4.3}$$

$$\omega > 0 \tag{4.4}$$

If these conditions are not satisfied, they likely cause numerical problems. Some turbulence models implicitly assume that the realizability conditions are satisfied. If this is not the case, division by zero or square roots of negative values may occur. This results in the simulation crashing. In addition, negative values in either k or ω may result in negative viscosity or wrong sign of dissipation terms. In turn, this affects the stability of the numerical method.

The Isogeometric Analysis (IgA) formulation of the k-ω equations does not guarantee positivity of k and/or ω. The turbulent equations are therefore modified to allow for negative working variables.

One approach is to use the logarithmic values of k and ω. This was introduced by Ilinca and Pelletier (1998) in the context of k-ε models. A benefit is that the equations for $\ln(k)$ and $\ln(\omega)$ are equivalent to the equations of k and ω. In addition, the distributions of $\ln(k)$ and $\ln(\omega)$ are also smoother than those of k and ω. Bassi et al. (2005) note that logarithmic of k may not be suitable for k-ω models that are integrated towards the wall. The boundary condition of k at the wall ($k = 0$) results in an infinite value for $\ln(k)$.

Bassi et al. (2005) used the logarithm of ω but not for k in a Discontinous Galerkin framework. To ensure positivity for k, they limited the value to zero. By applying appropriate substitutions they circumvented divisions by zero. In addition, they limited $\ln(\omega)$ in such a way that the realizability constraints of the Reynolds stresses are satisfied.

A similar approach is used by Stefanski et al. (2018), who also use the logarithm of ω but not for k. Inspired by the negative version of the Spallart-Allmaras model (Allmaras et al., 2012), they modified the equation for k. These modifications consists of an additional diffusion and source term that become active for negative values of k. Furthermore, instead of clipping the value of k, they use a differentiable ramp function. A lower limit for $\ln(\omega)$ is not used.

The approach in this thesis is based on the work of Bassi et al. (2005). A lower limit for $\ln(\omega)$ is not used as there is no easy analytical solution for this lower limit in an EARSM. First, the turbulent equations are restated for convience

$$\overline{u}_j \frac{\partial k}{\partial x_j} = \mathcal{P} - \beta^* k\omega + \frac{\partial}{\partial x_j}\left((\nu + \sigma_k \nu_T)\frac{\partial k}{\partial x_j}\right) \tag{4.5}$$

$$\overline{u}_j \frac{\partial \omega}{\partial x_j} = \gamma \frac{\omega}{k}\mathcal{P} - \beta\omega^2 + \frac{\partial}{\partial x_j}\left((\nu + \sigma_\omega \nu_T)\frac{\partial \omega}{\partial x_j}\right) + \sigma_d \frac{1}{\omega}\max\left(\frac{\partial k}{\partial x_j}\frac{\partial \omega}{\partial x_j}, 0\right) \tag{4.6}$$

The ω equation is transformed by introducing a new working variable $\tilde{\omega}$, which is related to ω via the transformation

$$\omega = e^{\tilde{\omega}} \tag{4.7}$$

The logarithmic version of the ω equation, i.e. the equation for $\tilde{\omega}$, is obtained by dividing Eq. 4.6 by ω and then substituting Eq. 4.7. This derivation is presented in Appendix A, and the result is

$$\overline{u}_j \frac{\partial \tilde{\omega}}{\partial x_j} = \gamma \frac{1}{k}\mathcal{P} - \beta e^{\tilde{\omega}} + \frac{\partial}{\partial x_j}\left((\nu + \sigma_\omega \nu_T)\frac{\partial \tilde{\omega}}{\partial x_j}\right) + (\nu + \sigma_\omega \nu_T)\frac{\partial \tilde{\omega}}{\partial x_j}\frac{\partial \tilde{\omega}}{\partial x_j} + \sigma_d e^{-\tilde{\omega}}\max\left(\frac{\partial k}{\partial x_j}\frac{\partial \tilde{\omega}}{\partial x_j}\right) \tag{4.8}$$

For the turbulent kinetic energy, Bassi et al. (2005) replaces k by a working variable $\tilde{k}$. In addition, a limited value $\overline{k}$ is introduced

$$\overline{k} = \max(\tilde{k}, 0) \tag{4.9}$$

The following equation for $\tilde{k}$ is then proposed

$$\overline{u_j}\frac{d\tilde{k}}{dx_j} = \mathcal{P} - \beta^* \overline{k}\omega + \frac{d}{dx_j}\left((\nu + \sigma_k \nu_T)\frac{d\tilde{k}}{dx_j}\right) \tag{4.10}$$

Where the working variable $\tilde{k}$ is used in the convective and diffusive terms, and the clamped value $\overline{k}$ in the production and dissipation terms to ensure the correct sign.

4.2. Production Limiter

In some stagnation regions there may be a large amount of turbulent buildup due to excessive turbulent production during iterations. To improve the stability of the numerical method, a production limiter is used. The production term in both the $\tilde{k}$ and $\tilde{\omega}$ equation is replaced by a clamped value.

$$\mathcal{P} \leftarrow \tilde{\mathcal{P}} = \min(\mathcal{P}, 10\beta^* \overline{k} e^{\tilde{\omega}}) \tag{4.11}$$

Which is based on the method used for the SST model by Menter et al. (2003). Menter et al. notes that in most applications the production to dissipation ratio ($\mathcal{P}/\varepsilon$) does not exceed 10. Thus, the final result should not be affected by this limiter.

4.3. Solution Procedure

The RANS equations, in combination with the $\tilde{k}$-$\tilde{\omega}$ equations, describe a steady state, coupled, non-linear problem. This generally a difficult problem to solve numerically. Various procedures have been proposed in literature to solve these equations.

For example, Codina and Soto (1999) used a segregated approach for a steady k-ε model. In this approach, the Navier-Stokes, k and ε are solved seperately in an iterative manner. The code used in thesis, DelFI, constructs a single large matrix for the entire system instead of seperate ones for each equation. Implementing a segregated procedure is therefore more diffucult. Instead, a different approach is used.

The opposite approach, which is used in this thesis, is to solve the coupled problem directly. This means that a single system to solve is constructed from the Navier-Stokes, $\tilde{k}$ and $\tilde{\omega}$ equations. Solving the steady state equations using this approach may be difficult, instead time continuation (or pseudo time integration) is used. The idea of this approach is to march a set of (pseudo-)transient equations towards steady state. The steady state solution is obtained as the time derivative vanishes.

Alternatively, this may be regarded as an implicit relaxation method. The change in solution variables is very small with a very small pseudo time step. Where the pseudo time step acts as a sort of relaxation parameter.

4.3.1. Time Integration in DelFi

DelFi is designed as a transient code for solving partial differential equations. For steady problems it is then natural to use a pseudo time approach, in which a solution is obtained by marching through pseudo time to a steady state. As a starting point, consider the discrete system obtained from the spatial discretization of the transport equations. In this thesis, this is the result of a Finite Element discretization. This pseudo time approach, however, is equally true for Finite Volume or Finite Difference discretizations

$$\mathbf{M}\dot{\mathbf{u}} + \mathbf{A}\mathbf{u} - \mathbf{f} = 0 \tag{4.12}$$

Here, $\mathbf{M}$ is the mass matrix, $\mathbf{A}$ is the result of discretizing the convection, diffusion and reaction terms and $\mathbf{f}$ contains source terms. The solution vector is $\mathbf{u}$ with its time derivative $\dot{\mathbf{u}}$. Note that for a non-linear system, $\mathbf{M}$, $\mathbf{A}$ and $\mathbf{f}$ may be functions of $\mathbf{u}$

$$\mathbf{M} = \mathbf{M}(\mathbf{u}) \quad \mathbf{A} = \mathbf{A}(\mathbf{u}) \quad \mathbf{f} = \mathbf{f}(\mathbf{u}) \tag{4.13}$$

Notice that Eq. 4.12 is an ordinary differential equation (ODE), which can be solved using time integration techniques. Such techniques are, for example, forward Euler, backward Euler and the family of Runge-Kutta methods. Backward Euler is used in this thesis, as it is unconditionally stable, yet relatively simple. The stability of the backward Euler method allows for larger time steps than of explicit methods such as forward Euler. As a result, steady state is reached sooner. There is, however, an increased cost of solving an implicit system, which is treated later on in this chapter. In the backward Euler method, the time derivative is approximated as

$$\dot{\mathbf{u}} = \frac{\mathbf{u}^{n+1} - \mathbf{u}^n}{\Delta t} \tag{4.14}$$

Where $\mathbf{u}^n$ is the solution at time iteration n, such that $t^n = t_0 + n\Delta t$, with t_0 being the start time (usually $t_0 = 0$) and Δt a time interval. And the approximation of Eq. 4.12 is

$$\mathbf{M}\dot{\mathbf{u}} + \mathbf{A}\mathbf{u}^{n+1} - \mathbf{f} = 0 \tag{4.15}$$

At this point, Eq. 4.14 is usually substituted in Eq. 4.15, resulting in a system that can be solved for $\mathbf{u}^{n+1}$. MFEM uses a different, but equivalent, procedure which allows a wide range of time integration techniques to be represented by the same interface in code. This procedure is derived for the backward Euler method by rewriting Eq. 4.14 as

$$\mathbf{u}^{n+1} = \mathbf{u}^n + \dot{\mathbf{u}}\Delta t \tag{4.16}$$

Which can be substituted in Eq. 4.15 to obtain

$$\mathbf{M}\dot{\mathbf{u}} + \mathbf{A}\left(\mathbf{u}^n + \dot{\mathbf{u}}\Delta t\right) - \mathbf{f} = 0 \tag{4.17}$$

And is a system that is solved for $\dot{\mathbf{u}}$

$$\left(\mathbf{M} + \mathbf{A}\Delta t\right)\dot{\mathbf{u}} = -\left(\mathbf{A}\mathbf{u}^n - \mathbf{f}\right) = -\mathbf{R}(\mathbf{u}^n) \tag{4.18}$$

Finally, Eq. 4.16 is used to obtain the solution $\mathbf{u}^{n+1}$. For linear partial differential equations, $\mathbf{M}$, $\mathbf{A}$ and $\mathbf{f}$ are constant and thus only a single system needs to be solved per time iteration. This is not the case for non-linear equations, where $\mathbf{M}$, $\mathbf{A}$ and $\mathbf{f}$ may be functions of $\mathbf{u}$. Denote $\mathbf{M}^n = \mathbf{M}(\mathbf{u}^n)$, $\mathbf{A}^n = \mathbf{A}(\mathbf{u}^n)$ and $\mathbf{f}^n = \mathbf{f}(\mathbf{u}^n)$, then the backward Euler approximation becomes

$$\mathbf{M}^{n+1}\dot{\mathbf{u}} + \mathbf{A}^{n+1}\left(\mathbf{u}^n + \dot{\mathbf{u}}\Delta t\right) - \mathbf{f}^{n+1} = 0 \tag{4.19}$$

Obviously, this system can not be solved in its current form as $\mathbf{M}^{n+1}$, $\mathbf{A}^{n+1}$ and $\mathbf{f}^{n+1}$ are unknown. An iterative procedure is used to solve for $\dot{\mathbf{u}}$. Specifically, Newton's method is used in this thesis. First, an approximation for $\dot{\mathbf{u}}$ is introduced: $\dot{\mathbf{u}} \approx \dot{\mathbf{u}}^k$. Where $\dot{\mathbf{u}}^k$ is the approximation at the k'th non-linear iteration. For convience, a temporal residual is defined

$$\mathbf{R}_t(\dot{\mathbf{u}}) = \mathbf{M}\dot{\mathbf{u}} + \mathbf{A}(\mathbf{u}^n + \dot{\mathbf{u}}\Delta t) - \mathbf{f} \tag{4.20}$$

Then a Taylor series is constructed for $\mathbf{R}_t(\dot{\mathbf{u}})$ at $\dot{\mathbf{u}}^k$

$$\mathbf{R}_t(\dot{\mathbf{u}}) = \mathbf{R}_t(\dot{\mathbf{u}}^k) + \frac{d\mathbf{R}_t(\dot{\mathbf{u}}^k)}{d\dot{\mathbf{u}}}\Delta\dot{\mathbf{u}}^{k+1} + \mathcal{O}\left(\left(\Delta\dot{\mathbf{u}}\right)^2\right) = 0 \tag{4.21}$$

Neglecting higher order terms, it is solved for the increment $\Delta\dot{\mathbf{u}}^{k+1} = \dot{\mathbf{u}}^{k+1} - \dot{\mathbf{u}}^k$

$$\frac{d\mathbf{R}_t(\dot{\mathbf{u}}^k)}{d\dot{\mathbf{u}}}\Delta\dot{\mathbf{u}}^{k+1} = -\mathbf{R}_t(\dot{\mathbf{u}}^k) \tag{4.22}$$

With the temporal residual $\mathbf{R}_t(\dot{\mathbf{u}}^k)$ given by

$$\begin{aligned}
\mathbf{R}_t(\dot{\mathbf{u}}^k) &= \mathbf{M}^k\dot{\mathbf{u}}^k + \mathbf{A}^k(\mathbf{u}^n + \dot{\mathbf{u}}^k\Delta t) - \mathbf{f}^k \\
\mathbf{M}^k &= \mathbf{M}(\mathbf{u}^n + \dot{\mathbf{u}}^k\Delta t) \\
\mathbf{A}^k &= \mathbf{A}(\mathbf{u}^n + \dot{\mathbf{u}}^k\Delta t) \\
\mathbf{f}^k &= \mathbf{f}(\mathbf{u}^n + \dot{\mathbf{u}}^k\Delta t)
\end{aligned} \tag{4.23}$$

The jacobian $\dfrac{d\mathbf{R}_t(\dot{\mathbf{u}}^k)}{d\dot{\mathbf{u}}}$ is then

$$\frac{d\mathbf{R}_t(\dot{\mathbf{u}}^k)}{d\dot{\mathbf{u}}^k} = \mathbf{M}^k + \mathbf{A}^k\Delta t \tag{4.24}$$

The new approximation $\dot{\mathbf{u}}^{k+1}$ is then computed from $\dot{\mathbf{u}}^{k+1} = \dot{\mathbf{u}}^k + \Delta\dot{\mathbf{u}}^{k+1}$. More commonly, the solution of iteration k and $k+1$ mixed. The update then becomes

$$\dot{\mathbf{u}}^{k+1} = \dot{\mathbf{u}}^k + \alpha^k\Delta\dot{\mathbf{u}}^{k+1} \tag{4.25}$$

Which is called explicit relaxation, where α^k is the relaxation factor. The non-linear procedure is summarised in Algorithm 1.

Algorithm 1 Time integration with constant Δt

$\mathbf{u}^n \leftarrow \mathbf{u}_0$
while $t^n \leq t^{end}$ **do**
  $\dot{\mathbf{u}}^k \leftarrow \mathbf{0}$
  while $||\mathbf{R}_t(\dot{\mathbf{u}}^k)|| > tolerance$ **do**
    $\mathbf{u}^k \leftarrow \mathbf{u}^n + \dot{\mathbf{u}}^k \Delta t$
    calculate $\mathbf{R}_t(\dot{\mathbf{u}}^k)$ and $\dfrac{d\mathbf{R}_t(\dot{\mathbf{u}}^k)}{d\dot{\mathbf{u}}}$ $using$ $\mathbf{u}^k$
    solve $\dfrac{d\mathbf{R}_t(\dot{\mathbf{u}}^k)}{d\dot{\mathbf{u}}} \Delta\dot{\mathbf{u}}^{k+1} = -\mathbf{R}_t(\dot{\mathbf{u}}^k)$
    $\dot{\mathbf{u}}^k \leftarrow \dot{\mathbf{u}}^k + \alpha^k \Delta\dot{\mathbf{u}}^{k+1}$
  end while
  $\mathbf{u}^n \leftarrow \mathbf{u}^n + \dot{\mathbf{u}}^k \Delta t$
  $t^n \leftarrow t^n + n\Delta t$
end while

In a finite element context, a similar procedure is used by Shakib et al. (1991) to solve the Navier-Stokes equations. Shakib et al. refers to this approach as a predictor-corrector scheme.

4.4. Solution Control

The update step for $\dot{\mathbf{u}}^{k+1}$ requires an explicit relaxation factor α^k. The approach taken in this thesis, is a line search algorithm. Such an algorithm seeks a relaxation factor that satisfies, minimize or maximize an objective. The objective in this thesis is to reduce the temporal residual $\mathbf{R}_t$ by a certain relative amount η_{nl} in each iteration

$$\frac{\mathbf{R}_t}{\mathbf{R}} \leq \eta_{nl} \tag{4.26}$$

The line search algorithm is summarised in Algorithm 2. The approach used, is to continuously half the relaxation factor till the desired reduction in residuals is achieved or if the relaxation falls below a certain threshold.

Algorithm 2 Line search algorithm for relaxation factor α^k

$\alpha^k = 1$
$\dot{\mathbf{u}} = \dot{\mathbf{u}}^k + \alpha^k \Delta\dot{\mathbf{u}}^{k+1}$
while $\mathbf{R}_t(\dot{\mathbf{u}}) > \eta_{nl}\mathbf{R}(\dot{\mathbf{u}}^k)$ **do**
  $\alpha^k \leftarrow \alpha^k/2$
  if $\alpha^k <$ $threshold$ **then**
    stop
  end if
  $\dot{\mathbf{u}} = \dot{\mathbf{u}}^k + \alpha^k \Delta\dot{\mathbf{u}}^{k+1}$
  compute $\mathbf{R}_t(\dot{\mathbf{u}})$
end while

The relaxation factor in turn controls a CFL number from which the pseudo time step is computed. If the relaxation factor is one, i.e. a full update, then the CFL number is doubled. If the relaxation factor falls below the threshold, then the CFL number is divided by 10.

5

Numerical Experiments

This chapter presents various test cases for verifying the implementation of the numerical method. The first three cases (Grad-Div Stabilisation, Homogeneous Isotropic Decaying Turbulence and Homogeneous Shear Flow) illustrate the performance of various components of the method. The final case evaluates the complete method on a turbulent Backward Facing Step.

5.1. Grad-Div Stabilisation

The Isogeometric Analysis formulation of the Navier-Stokes equations does not guarantee that the incompressibility condition is statisfied. Especially at higher Reynolds numbers, this became noticable in the linear solver. In this regime, the linear solver struggles with the continuity equation, resulting in an increased number of iterations. This may be improved by adding grad-div stabilisation.

The aim of this case is to test the robustness of Isogeometric Analysis formulation of the Navier-Stokes equations at high Reynolds number. This is done by comparing a formulation with and without grad-div stabilisation on the backward facing step. Quadratic NURBS elements are used for both the velocity and pressure fields. The Reynolds number based on the step height is $Re_H = 36000$. Note that a laminar model is used to focus on the Navier-Stokes equations, even though the flow is actually turbulent. The resulting flowfield is therefore not accurate. In addition, the mesh is relatively coarse with 4841 degrees of freedom per variable.

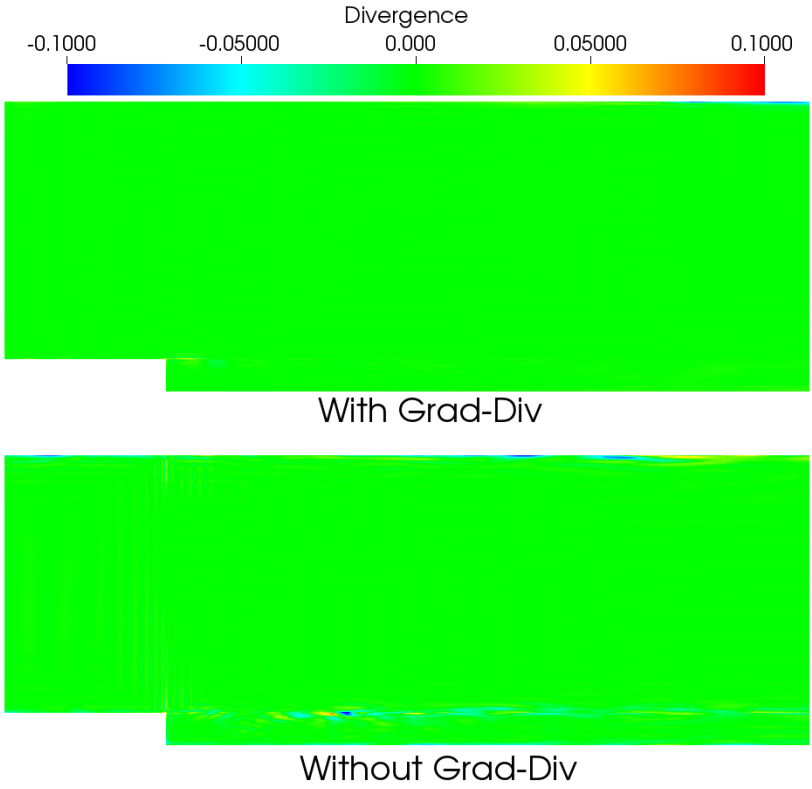

Figure 5.1: Divergence field for $Re_H = 36000$, using a laminar model. Top image is with Grad-Div stabilisation, bottom image is without Grad-Div stabilisation.

The normalized divergence field near the step is shown in Figure 5.1. Notice here that the grad-div formulation results in a much smoother field compared to the formulation without grad-div stabilisation. Especially in the wake of the step, there a various spots which are not divergence free for the formulation without grad-div stabilisation.

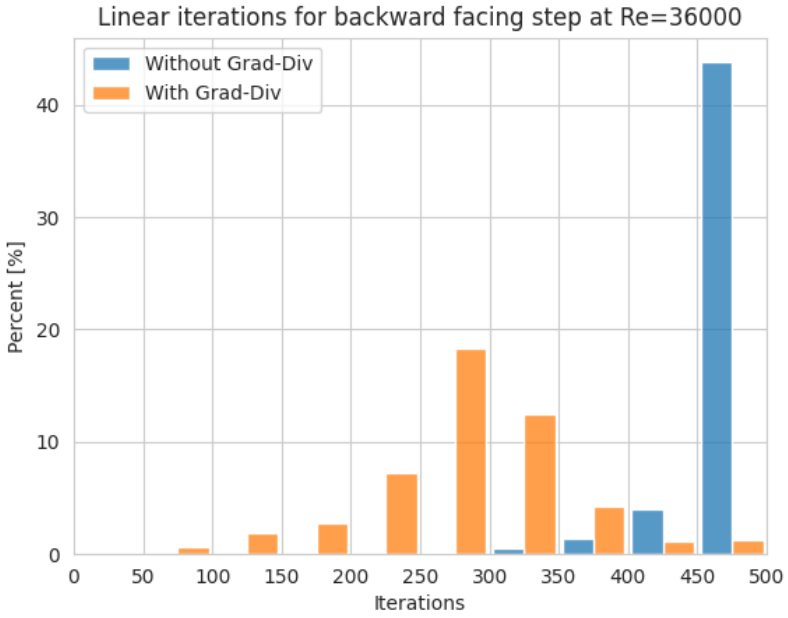

Figure 5.2: Distribution of number of linear iterations needed. Grad-Div stabilisation requires less linear iterations at high Reynolds number

The effect of the grad-div formulation on the performance of the linear solver is shown in Figure 5.2. This figure illustrates the distribution of iterations needed. Most notably, the formulation without grad-div stabilisation requires a lot of linear iterations, 450 - 500 iterations, for most of the time. Where 500 iterations where the specified maximum number of iterations. The formulation with grad-div stabilisation, on the other hand, requires on average 250 - 350 iterations. Thus grad-div stabilisation results in less computational effort.

Thus the grad-div stabilisation results in both a better divergence field, and less computational effort. All following computations have therefore been done using grad-div stabilisation.

5.2. Homogeneous Isotropic Decaying Turbulence

The goal of this case is to verify the linearisation of the dissipation terms in the $\tilde{k}$-$\tilde{\omega}$ equations. In this thesis, the dissipation terms are treated explicitly. This means they are taken as part of the source vector and thus have no contribution to the jacobian in the non-linear solver.

The case considered here is homogeneous isotropic decaying turbulence. Instead of using the model by Hellsten (2005), the k-ω model of Wilcox (1988) is used here. This model has constant coefficients, for which an analytical solution exists. For k and ω these are

$$\omega = \frac{1}{\beta t + \frac{1}{\omega_0}} \tag{5.1}$$

$$k = \frac{k_0}{\omega_0^{\beta^*/\beta}} \left(\beta t + \frac{1}{\omega_0} \right)^{-\beta^*/\beta} \tag{5.2}$$

With k_0 and ω_0 being the initial conditions. This case is simulated on a unit square domain with quadratic NURBS elements. Figure 5.3 shows the decay of k and ω. The simulated and analytical results match well. Thus the linearisation of the dissipation terms functions as expected when $\tilde{k}$ and $\tilde{\omega}$ are positive.

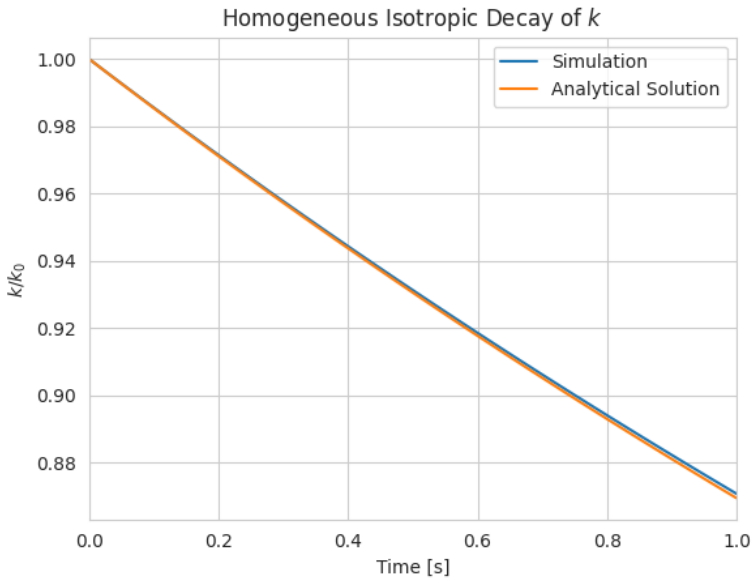

(a) Decay of turbulent kinetic energy

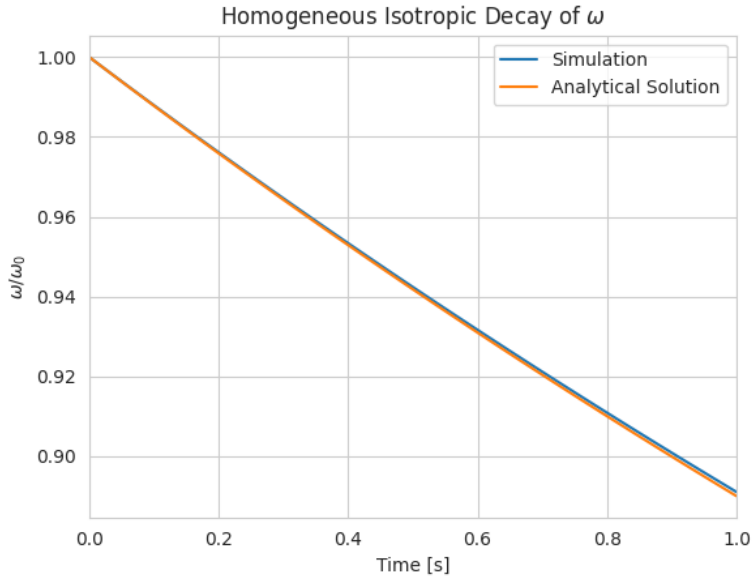

(b) Decay of specific turbulent dissipation rate

Figure 5.3: Comparision of simulation and analytical solution for the decay of k and ω in homogeneous isotropic turbulence

5.3. Homogeneous Shear Flow

This case may be regarded as a continuation of homogeneous isotropic decaying turbulence, in that production terms are now included in addition to dissipation terms. In this case, the horizontal velocity component varies lineary in vertical direction, so that the only velocity gradient present is $\frac{\partial \overline{u}}{\partial y} = S$. The k-ω equations then reduce to

$$\frac{\partial \omega}{\partial t} = \gamma S^2 - \beta^* \omega^2 \tag{5.3}$$

$$\frac{\partial k}{\partial t} = \frac{k}{\omega} S^2 - \beta^* k \omega \tag{5.4}$$

The analytical solution for ω is

$$\omega = \sqrt{\frac{\gamma S^2}{\beta}} \tanh(\sqrt{\gamma\beta S^2}(c_1 + t)) \tag{5.5}$$

With

$$c_1 = \frac{1}{\sqrt{\gamma\beta S^2}} \arctan(\omega_0 \sqrt{\frac{\beta}{\gamma S^2}}) \tag{5.6}$$

With the analytical solution for ω, a solution may be derived for k. This is, however, quite a bit more difficult and is not presented here.

The simulation is again carried out on a unit square domain with quadratic NURBS elements. The comparison between the analytical and simulated solution is shown in Figure 5.4. The results match well. The production term in the $\tilde{\omega}$ equation thus performs as expected for positive values of $\tilde{k}$ and $\tilde{\omega}$.

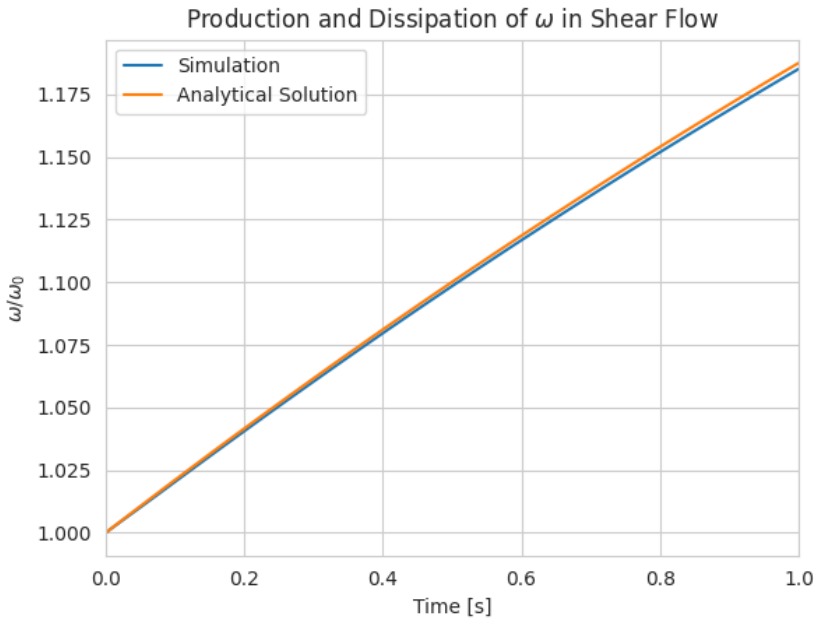

Figure 5.4: Comparison for ω in homogeneous shear flow between analytical and simulated solution

5.4. Backward Facing Step

The test case considered is the backward facing step. It is common test case for turbulent flow simulations. It features forced seperation from the step with reattachment downstream, thus forming a recirculation zone. Performance of turbulence models in this case are generally judged on their ability to predict the reattachment point, velocity profiles, Reynolds stress profiles and drag and pressure coefficients.

5.4.1. Case description

The geometry consists of a step with height 1, preceded by a channel with length $L/H = 110$. The length of this channel is chosen so that a boundary layer may form naturally. Alternatively, some studies use a channel with length $L/H = 4$ and then prescribe (experimental) velocity profiles at the inlet. This method is not used in this thesis as profiles for the turbulent quantities k and ω are not readily available. The step is followed by a channel of length $L/H = 50$. The reattachement point found in experimental studies was $x/H = 6.26$ based on skin friction. Therefore, it is expected that this channel is long enough.

The mesh consists of a region of uniform elements for $0 \leq x/H \leq 10$, which is longer than the experimental recirculation. The mesh is stretched in the x direction for $x/H < 0$ & $x/H > 10$.

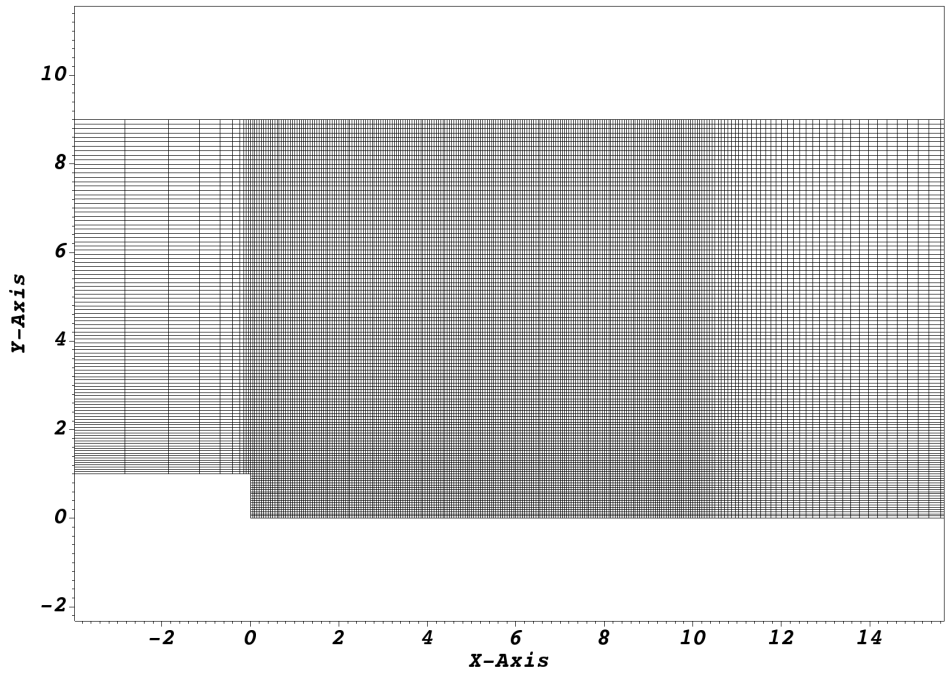

Figure 5.5: Mesh near backward step

5.4.2. Effect of Artificial Diffusion

While doing the calculations for the backward facing step, it became apparent that the stabilised formulation by itself did not result in a converging method. The weak formulation for the Navier-Stokes, k and $ln(\omega)$ are each therefore supplemented by an additional stabilising term, which is implemented as isotropic diffusion. The formulation for the stabilising viscosity is restated for convience

$$\tilde{\nu} = C_{rb}h^2||R|| + C_{ic}||u||h \tag{5.7}$$

Note that this viscosity consists of a consistent term ($C_{rb}h^2||R||$) and an inconsistent term ($C_{ic}||u||h$). With an inconsistent term, one wishes for the least amount of artificial diffusion while still having a converging method. Three pairs of coefficients are therefore investigated $(C_{rb}, C_{ic}) = (1.0, 0.5)$, $(0.5, 0.25)$, $(0.25, 0.125)$. The residual history for each coefficient pair is shown in Figure 5.6 & 5.7. Note that for $C_{rb} = 0.25$ & $C_{ic} = 0.125$, with a Reynolds number of $Re_H = 20000$, the residuals do not converge (See Figure 5.6c). At a higher Reynolds number, $Re_H = 36000$, only the most diffusive case converges (See Figure 5.7a). This indicates that there is some minimal amount of artificial diffusion required for the implementation to be convergent. Moreover, the ”optimal” set of parameters is dependent on the Reynolds number.

The current method is convergent for the other two coefficient pairs at $Re_H = 20000$ and one set at $Re_H = 36000$. These cases display a general outline for the residuals: in the first few iterations, all residuals except for k decrease by about an order of magnitude. This is followed by a ”plateau”, whose duration is dependent on the artificial diffusion. In the mean time, the residual for k increases by about three to four orders of magnitude. After which, all residuals start trending downward.

The residuals in Figure 5.6 & 5.7 indicate that the overall convergence issues arise from the k-equation. The ability of the numerical method to overcome sudden increases of the residual of k appears crucial. It is important to note that an increase in residuals of k is not uncommon. It is also observed by Stefanski et al. (2018) in their formulation of Wilcox's k-ω model.

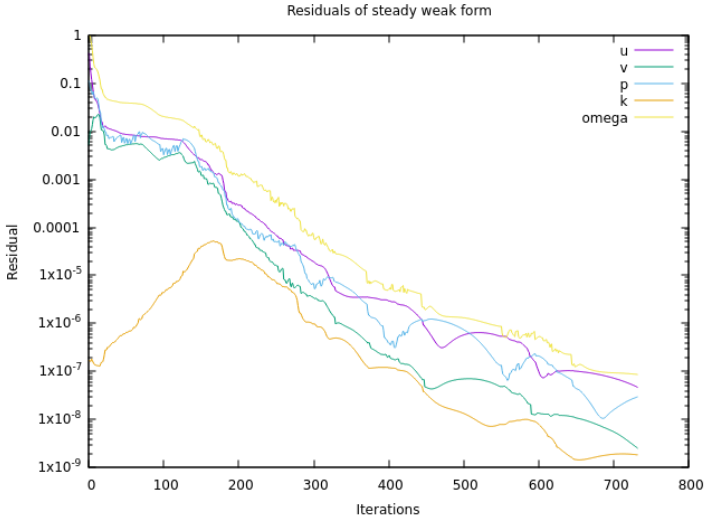

(a) $C_{rb} = 1$, $C_{ic} = 0.5$

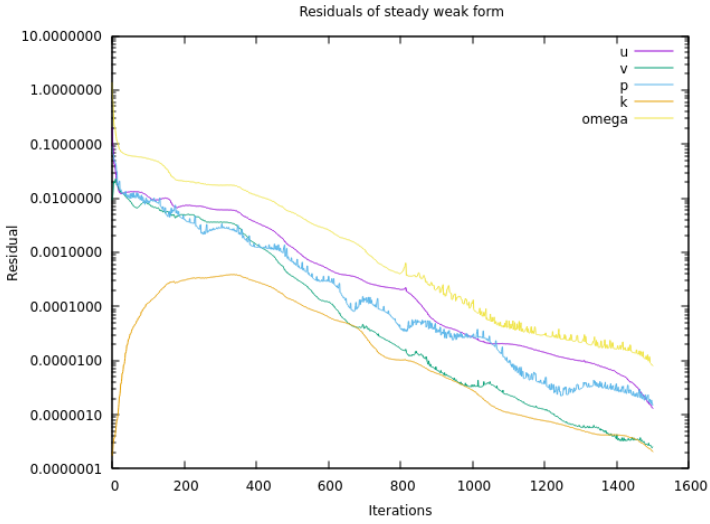

(b) $C_{rb} = 0.5$, $C_{ic} = 0.25$

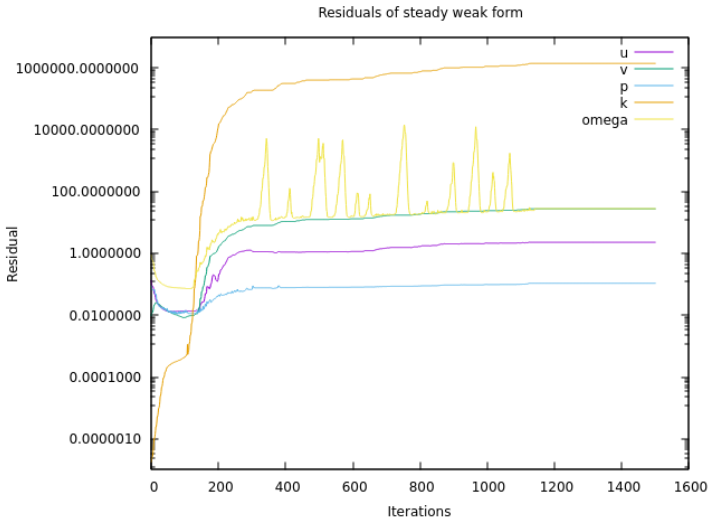

(c) $C_{rb} = 0.25$, $C_{ic} = 0.125$

Figure 5.6: Residual history of u, v, p, $\tilde{k}$, $ln(\omega)$. $Re_H = 20000$

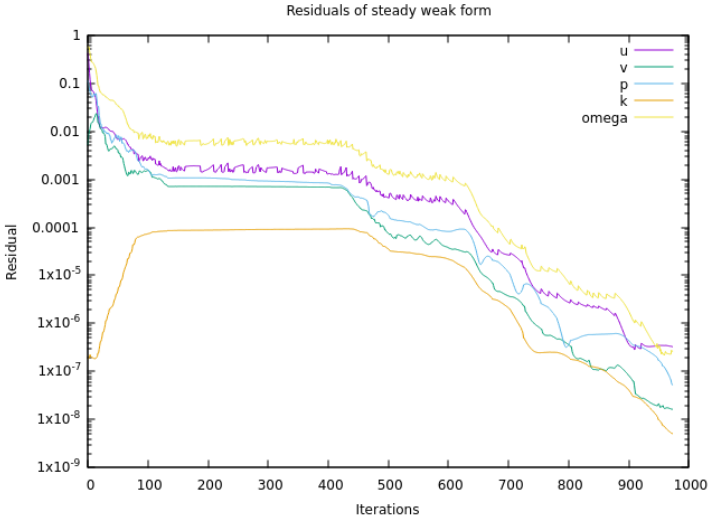

(a) $C_{rb} = 1$, $C_{ic} = 0.5$

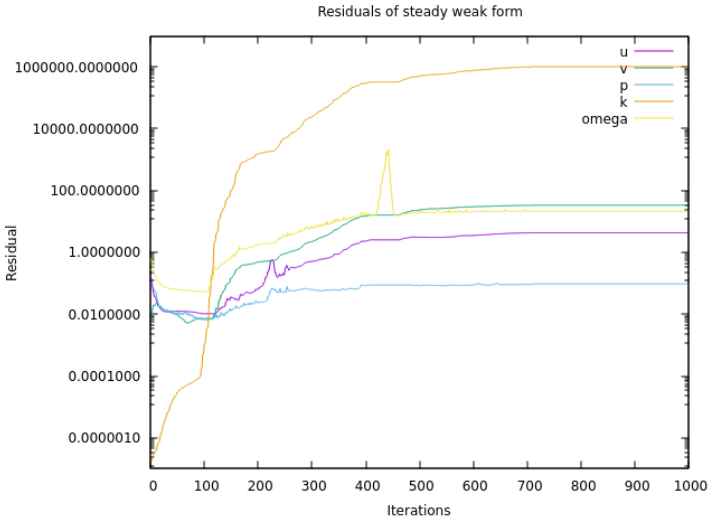

(b) $C_{rb} = 0.5$, $C_{ic} = 0.25$

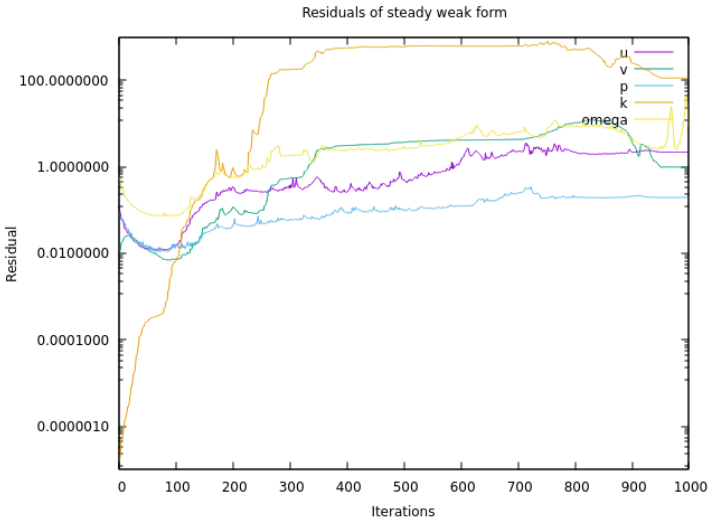

(c) $C_{rb} = 0.25$, $C_{ic} = 0.125$

Figure 5.7: Residual history of u, v, p, $\tilde{k}$, $ln(\omega)$. $Re_H = 36000$

From testing it appears that difficulties originate from the production and dissipation terms in the k equation. Ommitting these terms results in a linearised convection-diffusion equation in this formulation, which converges without issue. During testing it was unclear whether this was due to the reactive nature, coupling of k-ω equations or their interaction in regions with a negative working variable.

The problems in the k equation are further illustrated in Figure 5.8. At iteration 100, the point at which k starts diverging, there is unphysical behaviour present in the field of $\tilde{k}$, while u remains a smooth field. This unphysical effect is, however, propegates throughout the iterations. At iteration 1000, there is a completely unphysical field for k. This effect is then also noticed in the velocity. A lot of numerical artefacts appear in the velocity field near the step, wich correspond to the area of unphysical behaviour in $\tilde{k}$. Again, it appears that these artefacts are due to the unrealistic field of $\tilde{k}$.

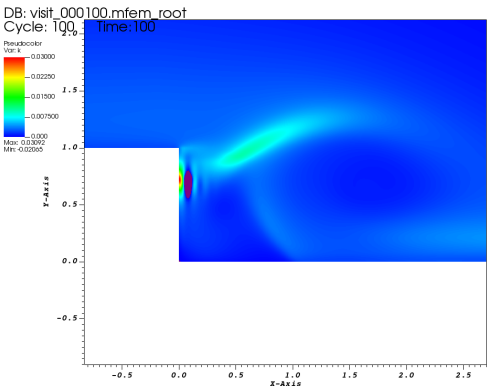

(a) $\tilde{k}$ at iteration 100. Note the presence of (unphysical) oscilliations at the top half of the step.

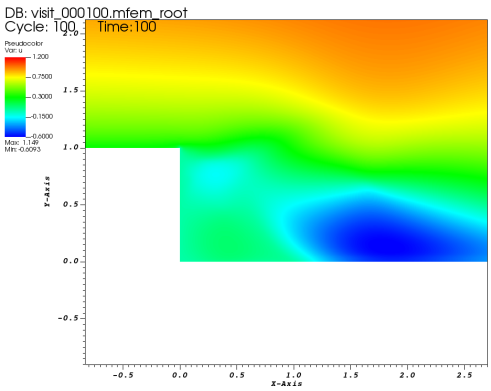

(b) u at iteration 100. The velocity field is still smooth

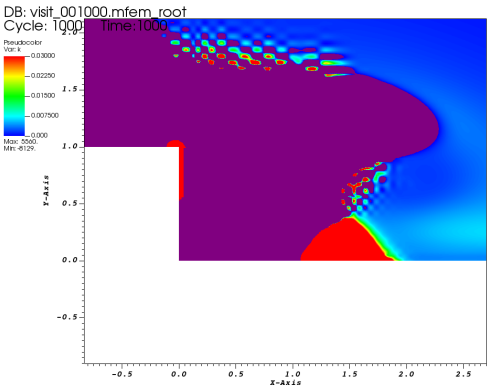

(c) $\tilde{k}$ at iteration 1000. The immediate area around the step is dominated by an unphysical field.

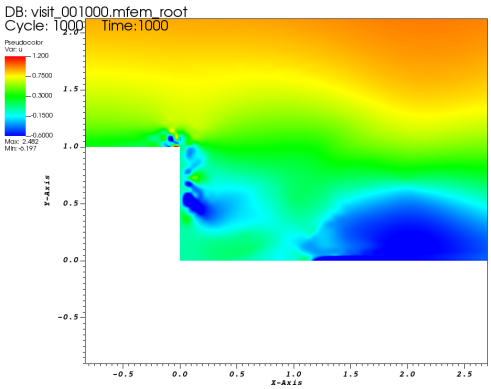

(d) u at iteration 1000. Note the unphysical behaviour near the step.

Figure 5.8: Horizontal velocity and turbulent kinetic energy field at iterations 100 and 1000 of the simulation.

5.4.3. Effect of initial CFL number

The solution procedure uses a time step that acts as a relaxation parameter that is controlled by a CFL number. An important consideration herein is that it should be sufficiently small in the first few iterations to prevent strong transients. This may however result in smaller CFL values throughout, slowing convergence. Figure 5.9 shows the CFL history for $Re_H = 36000$ for various initial CFL values. From the figure it can be seen that the iteration process remains largely unaffected by the initial CFL value. Therefore, a small (CFL = 0.1) inital value is used throughout the remainder of this chapter. This does not affect the solution process overall, and results in small changes within the first few iterations.

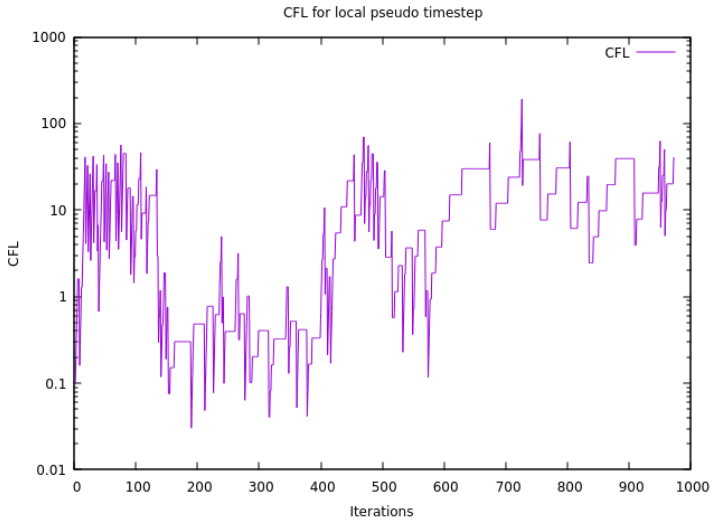

(a) CFL = 0.1

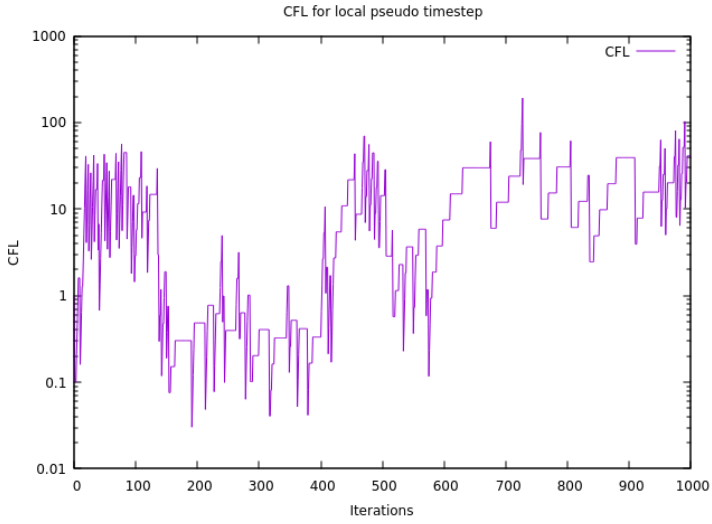

(b) CFL = 1

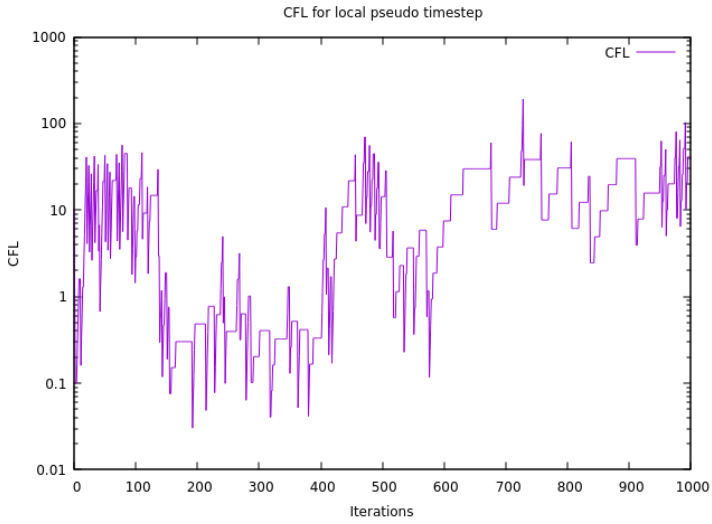

(c) CFL = 10

Figure 5.9: Effect of initial CFL value on iteration process

5.4.4. Validation

The resulting fields for u, k and ω are shown in Figure 5.10. The Reynolds number based on the step height is $Re_H = 36000$. The case with most artificial diffusion is shown here as it was the only converged solution. Comparing k and ω to similar simulations, such as those by Stefanski et al. (2018), it is noted that the k is much more spread out. Especially as it progresses downstream. This is expected, due to the added artificial diffusion. In addition, the area of maximum kinetic energy is farther downstream (starting at $x/H \approx 5$). The specific dissipation rate is a similar case. Qualitaviley, the fields are comparable, albeit more diffusive.

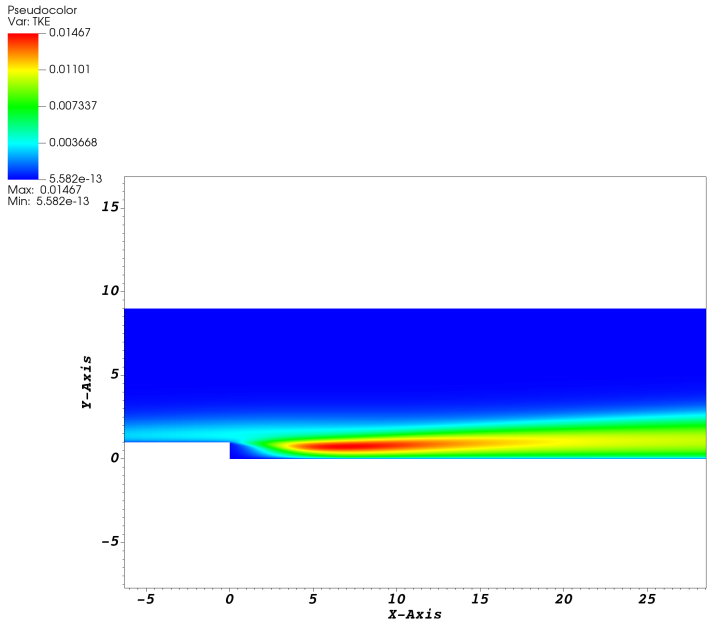

(a) Turbulent kinetic energy field

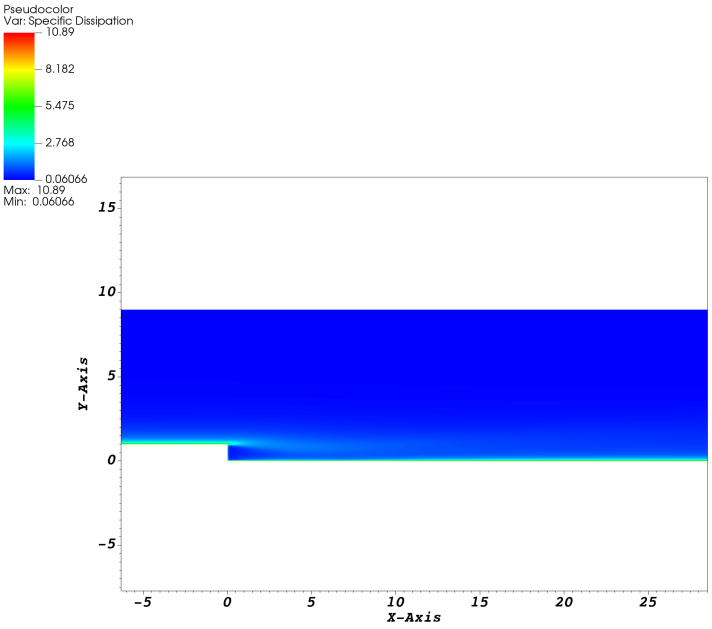

(b) Turbulent specific dissipation field

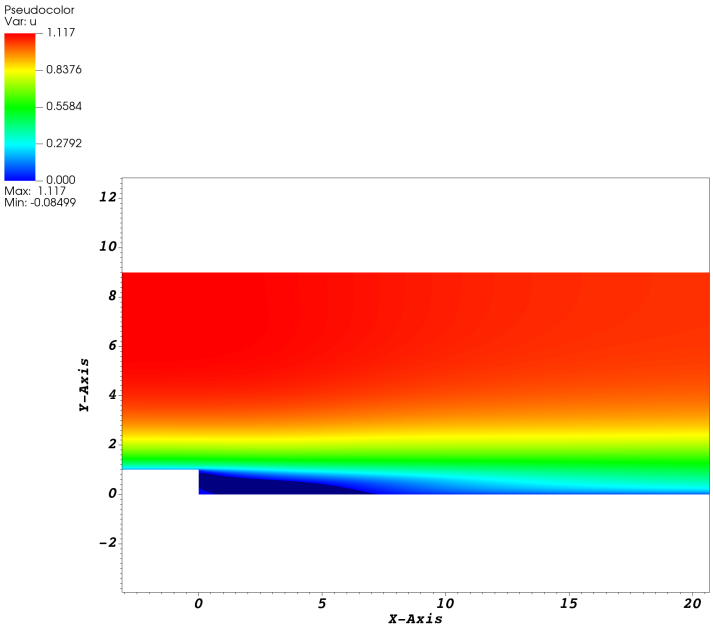

(c) Horizontal velocity field

Figure 5.10: Fields of various variables

The diffusive effect is especially apparent in the velocity field. At this Reynolds number, it is expected that the top of the boundary layer ”moves” downward. Here, the outer region remains more or less at the same y coordinate. The effect is also apparent by comparing the velocity profile upstream of the step to experimental values, see Figure 5.11. Here it is seen that that the boundary layer thickness is much larger than the measured profile.

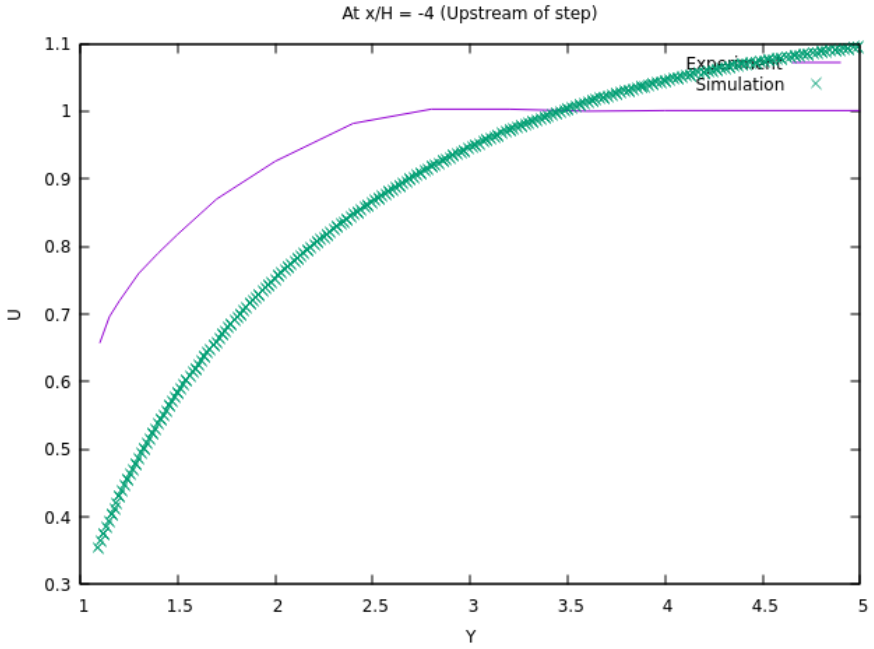

Figure 5.11: Velocity profile at inlet

6

Conclusion

The objective of this thesis was to implement, verify and validate an Explicit Algebraic Reynolds Stress Model using a stabilised Isogeometric Analysis formulation for seperated flow near a rounded transom intercepter. The Explicit Algebraic Reynolds Stress model of Wallin and Johansson (2000) is implemented using the full integrity basis in 2D, in combination with a k-ω model from Hellsten (2005) whose coefficients are tuned for this particular EARSM.

The Navier-Stokes equations are stabilised with SUPG, PSPG, Grad-Div and both consistent and inconsistent artificial diffusion. The turbulent equations are transformed to allow for negative values. In addition, a production limiter is used to prevent a buildup of turbulence. The turbulent equations are stabilised using SUPG and artificial diffusion. A pseudo time formulation with artificial diffusion is used to advance the coupled equations through pseudo time.

The implemented model is not tested near a rounded transom interceptor. Verification with the backward facing step at $Re_H = 36000$ showed that the current formulation without artificial diffusion was unstable. The addition of artificial diffusion ($C_{rb} = 1$, $C_{ic} = 0.5$) was necessary to obtain a converged solution. The results are overly diffusive, and not accurate. Validation for a transom intercepter was therefore not performed.

Numerical difficulties arise in the negative version of the k equation. For the backward facing step, numerical artefacts appear first in the turbulent kinetic energy before any other field. Which become worse as the iteration proceeds. The dissipation term in the k equation and production and dissipation term in the $ln(\omega)$ perform as expected with constant coefficients in simple test cases. Potential causes may then be the production term in the k equation, interaction (or lack thereof) with negative values or the non-linear coefficients in the k-ω model.

The time step in the solution procedure is computed based on CFL number. The solution procedure was insensitive to the initial value of this CFL number. Within a few iterations, almost identical time histories were obtained.

Due to the artificial diffusion required for a stable method, the results of the backward facing step show significant errors compared to experimental results. The displacement thickness of the boundary layer is significant larger than expected. Qualitaviley, some similarities are observed with another stabilised finite element approach. Showing increased turbulence downstream of the step. These were, however, further downstream due to the artificial diffusion.

6.1. Recommedations

The main recommedation for further work is to improve the stability of the negative version of the kinetic energy equation. Points of interest are: 1) the production term in the k equation. Instead of using the full definition of an EARSM with a limiter, it may be approximated. 2) Inclusion of additional terms that force $\tilde{k}$ towards positive values. These may be source like terms if $\tilde{k}$ is negative, or increased viscosity for negative values of $\tilde{k}$. See Stefanski et al. (2018), for example. 3) Freezing certain quantities, such as turbulent production, during iterations (See Codina and Soto (1999)). This may minimise effects due to large gradients from over- and undershoot near boundaries.

The next step towards validation with a rounded transom interceptor is to verify the performance for cases with curved surfaces. Such as a periodic hill or Stratford ramp. After which a rounded transom interceptor may be validated.

A

Transformation of ω Equation

This appendix presents the derivation of the logarithmic version of the turbulent ω equation. Also referred to as the equation for the working variable $\tilde{\omega}$. This working variable is related to ω via the transformation

$$\omega = e^{\tilde{\omega}} \tag{A.1}$$

The starting point for the derivation of the $\tilde{\omega}$ equation is the usual turbulent equation for ω

$$\overline{u}_j \frac{\partial \omega}{\partial x_j} = \gamma \frac{\omega}{k} \mathcal{P} - \beta \omega^2 + \frac{\partial}{\partial x_j}\left((\nu + \sigma_\omega \nu_T) \frac{\partial \omega}{\partial x_j} \right) + \sigma_d \frac{1}{\omega} \max\left(\frac{\partial k}{\partial x_j} \frac{\partial \omega}{\partial x_j}, 0 \right) \tag{A.2}$$

The first step is to divide Eq. A.2 by ω, resulting in

$$\overline{u}_j \frac{1}{\omega} \frac{\partial \omega}{\partial x_j} = \gamma \frac{1}{k} \mathcal{P} - \beta \omega + \frac{1}{\omega} \frac{\partial}{\partial x_j}\left((\nu + \sigma_\omega \nu_T) \frac{\partial \omega}{\partial x_j} \right) + \sigma_d \frac{1}{\omega^2} \max\left(\frac{\partial k}{\partial x_j} \frac{\partial \omega}{\partial x_j}, 0 \right) \tag{A.3}$$

Next, Eq. A.1 is substituted in Eq. A.3

$$\overline{u}_j e^{-\tilde{\omega}} \frac{\partial e^{\tilde{\omega}}}{\partial x_j} = \gamma \frac{1}{k} \mathcal{P} - \beta e^{\tilde{\omega}} + e^{-\tilde{\omega}} \frac{\partial}{\partial x_j}\left((\nu + \sigma_\omega \nu_T) \frac{\partial e^{\tilde{\omega}}}{\partial x_j} \right) + \sigma_d e^{-2\tilde{\omega}} \max\left(\frac{\partial k}{\partial x_j} \frac{\partial e^{\tilde{\omega}}}{\partial x_j}, 0 \right) \tag{A.4}$$

This equation, with use of the chain rule and simplification, results in the final form for $\tilde{\omega}$. The following sections show the simplification for the convection, diffusion and cross-diffusion terms respectively.

A.1. Convection Term

The first step for the convection term is to use the chain rule

$$\overline{u}_j e^{-\tilde{\omega}} \frac{\partial e^{\tilde{\omega}}}{\partial x_j} = \overline{u}_j e^{-\tilde{\omega}} \frac{\partial e^{\tilde{\omega}}}{\partial \tilde{\omega}} \frac{\partial \tilde{\omega}}{\partial x_j} \tag{A.5}$$

Which can be simplified to

$$\overline{u}_j e^{-\tilde{\omega}} \frac{\partial e^{\tilde{\omega}}}{\partial \tilde{\omega}} \frac{\partial \tilde{\omega}}{\partial x_j} = \overline{u}_j e^{-\tilde{\omega}} e^{\tilde{\omega}} \frac{\partial \tilde{\omega}}{\partial x_j} = \overline{u}_j \frac{\partial \tilde{\omega}}{\partial x_j} \tag{A.6}$$

A.2. Diffusion Term

First, apply the chain rule to the diffusion term

$$e^{-\tilde{\omega}} \frac{\partial}{\partial x_j}\left((\nu + \sigma_\omega \nu_T) \frac{\partial e^{\tilde{\omega}}}{\partial x_j} \right) = e^{-\tilde{\omega}} \frac{\partial}{\partial x_j}\left((\nu + \sigma_\omega \nu_T) \frac{\partial e^{\tilde{\omega}}}{\partial \tilde{\omega}} \frac{\partial \tilde{\omega}}{\partial x_j} \right) = e^{-\tilde{\omega}} \frac{\partial}{\partial x_j}\left((\nu + \sigma_\omega \nu_T) e^{\tilde{\omega}} \frac{\partial \tilde{\omega}}{\partial x_j} \right) \tag{A.7}$$

Which may be written as two terms using the product rule

$$\begin{aligned} e^{-\tilde{\omega}} \frac{\partial}{\partial x_j} \left((\nu + \sigma_\omega \nu_T) e^{\tilde{\omega}} \frac{\partial \tilde{\omega}}{\partial x_j} \right) &= e^{-\tilde{\omega}} (\nu + \sigma_\omega \nu_T) \frac{\partial e^{\tilde{\omega}}}{\partial x_j} \frac{\partial \tilde{\omega}}{\partial x_j} + e^{-\tilde{\omega}} e^{\tilde{\omega}} \frac{\partial}{\partial x_j} \left((\nu + \sigma_\omega \nu_T) \frac{\partial \tilde{\omega}}{\partial x_j} \right) \\ &= e^{-\tilde{\omega}} (\nu + \sigma_\omega \nu_T) \frac{\partial e^{\tilde{\omega}}}{\partial x_j} \frac{\partial \tilde{\omega}}{\partial x_j} + \frac{\partial}{\partial x_j} \left((\nu + \sigma_\omega \nu_T) \frac{\partial \tilde{\omega}}{\partial x_j} \right) \end{aligned} \tag{A.8}$$

Lastly, applying the chain rule once more and simplyfying the result

$$\begin{aligned} &e^{-\tilde{\omega}} (\nu + \sigma_\omega \nu_T) \frac{\partial e^{\tilde{\omega}}}{\partial x_j} \frac{\partial \tilde{\omega}}{\partial x_j} + \frac{\partial}{\partial x_j} \left((\nu + \sigma_\omega \nu_T) \frac{\partial \tilde{\omega}}{\partial x_j} \right) = \\ &e^{-\tilde{\omega}} (\nu + \sigma_\omega \nu_T) \frac{\partial e^{\tilde{\omega}}}{\partial \tilde{\omega}} \frac{\partial \tilde{\omega}}{\partial x_j} \frac{\partial \tilde{\omega}}{\partial x_j} + \frac{\partial}{\partial x_j} \left((\nu + \sigma_\omega \nu_T) \frac{\partial \tilde{\omega}}{\partial x_j} \right) = \\ &e^{-\tilde{\omega}} e^{\tilde{\omega}} (\nu + \sigma_\omega \nu_T) \frac{\partial \tilde{\omega}}{\partial x_j} \frac{\partial \tilde{\omega}}{\partial x_j} + \frac{\partial}{\partial x_j} \left((\nu + \sigma_\omega \nu_T) \frac{\partial \tilde{\omega}}{\partial x_j} \right) = \\ &(\nu + \sigma_\omega \nu_T) \frac{\partial \tilde{\omega}}{\partial x_j} \frac{\partial \tilde{\omega}}{\partial x_j} + \frac{\partial}{\partial x_j} \left((\nu + \sigma_\omega \nu_T) \frac{\partial \tilde{\omega}}{\partial x_j} \right) \end{aligned} \tag{A.9}$$

In summary, the diffusion term may be written As

$$\begin{aligned} &e^{-\tilde{\omega}} \frac{\partial}{\partial x_j} \left((\nu + \sigma_\omega \nu_T) \frac{\partial e^{\tilde{\omega}}}{\partial x_j} \right) = \\ &(\nu + \sigma_\omega \nu_T) \frac{\partial \tilde{\omega}}{\partial x_j} \frac{\partial \tilde{\omega}}{\partial x_j} + \frac{\partial}{\partial x_j} \left((\nu + \sigma_\omega \nu_T) \frac{\partial \tilde{\omega}}{\partial x_j} \right) \end{aligned} \tag{A.10}$$

A.3. Cross-Diffusion Term

For the cross-diffusion term, the first step is to apply the chain rule to the dot product in the max function

$$\begin{aligned} \sigma_d e^{-2\tilde{\omega}} \max \left(\frac{\partial k}{\partial x_j} \frac{\partial e^{\tilde{\omega}}}{\partial x_j}, 0 \right) &= \sigma_d e^{-2\tilde{\omega}} \max \left(\frac{\partial k}{\partial x_j} \frac{\partial e^{\tilde{\omega}}}{\partial \tilde{\omega}} \frac{\partial \tilde{\omega}}{\partial x_j}, 0 \right) \\ &= \sigma_d e^{-2\tilde{\omega}} \max \left(e^{\tilde{\omega}} \frac{\partial k}{\partial x_j} \frac{\partial \tilde{\omega}}{\partial x_j}, 0 \right) \end{aligned} \tag{A.11}$$

Note that the $e^{\tilde{\omega}}$ term inside the max function is strictly positive. It can therefore be taken outside the function without altering the result

$$\max \left(e^{\tilde{\omega}} \frac{\partial k}{\partial x_j} \frac{\partial \tilde{\omega}}{\partial x_j}, 0 \right) = e^{\tilde{\omega}} \max \left(\frac{\partial k}{\partial x_j} \frac{\partial \tilde{\omega}}{\partial x_j}, 0 \right) \tag{A.12}$$

Thus, the cross-diffusion term may be written as

$$\begin{aligned} \sigma_d e^{-2\tilde{\omega}} \max \left(\frac{\partial k}{\partial x_j} \frac{\partial e^{\tilde{\omega}}}{\partial x_j}, 0 \right) &= \sigma_d e^{-2\tilde{\omega}} e^{\tilde{\omega}} \max \left(\frac{\partial k}{\partial x_j} \frac{\partial \tilde{\omega}}{\partial x_j}, 0 \right) \\ &= \sigma_d e^{-\tilde{\omega}} \max \left(\frac{\partial k}{\partial x_j} \frac{\partial \tilde{\omega}}{\partial x_j}, 0 \right) \end{aligned} \tag{A.13}$$

A.4. Logarithmic Equation for ω

B

Weak Form Equations

$$
\begin{aligned}
&\left(w_i, \frac{du_i}{dt} + u_j \frac{du_i}{dx_j}\right)_\Omega + \left(\frac{dw_i}{dx_j}, (\nu + \nu_T)\left(\frac{du_i}{dx_j} + \frac{du_j}{dx_i}\right) - p - a_{ij}^{(ex)} k\right)_\Omega + \left(q, \frac{du_j}{dx_j}\right)_\Omega \\
&+ \left(\tau u_j \frac{dw_i}{dx_j}, u_k \frac{du_i}{dx_k} + \frac{dp}{dx_i}\right)_\Omega + \left(\tau \frac{dq}{dx_i}, u_j \frac{du_i}{dx_j} + \frac{dp}{dx_i}\right)_\Omega + \left(\frac{dw_i}{dx_j}, \nu_{DC} \frac{du_i}{dx_j}\right)_\Omega \\
&- \left(w_i, (\nu + \nu_T) n_j \left(\frac{du_i}{dx_j} + \frac{du_j}{dx_i}\right)\right)_{\Gamma_{wall}} + \left(w_i, n_i p\right)_{\Gamma_{wall}} + \left(w_i, a_{ij}^{(ex)} n_j k\right)_{\Gamma_{wall}} \\
&- \left(\frac{dw_i}{dx_j}, (\nu + \nu_T) n_j u_i\right)_{\Gamma_{wall}} + \left(C_b w_i, u_i\right)_{\Gamma_{wall}} - \left(q, u_j n_j u_i\right)_{\Gamma_{wall}} \\
&- \left(w, u_j n_j u_i\right)_{\Gamma_{backflow}} \\
&- \left(w, 0\right)_{\Gamma_{outflow}} \\
&= 0
\end{aligned}
\tag{B.1}
$$

$$
\begin{aligned}
&\left(w, \frac{d\tilde{k}}{dt} + u_j \frac{d\tilde{k}}{dx_j} - \tilde{P} + \beta^* \omega \bar{k}\right)_\Omega + \left(\frac{dw}{dx_j}, (\nu + \sigma_k \nu_T) \frac{d\tilde{k}}{dx_j}\right)_\Omega \\
&+ \left(\tau u_j \frac{dw}{dx_j}, u_j \frac{d\tilde{k}}{dx_j} - \tilde{P} + \beta^* \omega\right)_\Omega + \left(\frac{dw}{dx_j}, \nu_{DC,k} \frac{d\tilde{k}}{dx_j}\right)_\Omega \\
&- \left(w, (\nu + \sigma_k \nu_T) n_j \frac{d\tilde{k}}{dx_j}\right)_{\Gamma_{wall}} - \left(\frac{dw}{dx_j}, (\nu + \sigma_k \nu_T) n_j (\tilde{k} - g_\omega)\right)_{\Gamma_{wall}} + \left(C_b w, \tilde{k} - g_\omega\right)_{\Gamma_{wall}} \\
&- \left(w, u_j n_j (\tilde{k} - \tilde{k}_\infty)\right)_{\Gamma_{backflow}} \\
&- \left(w, 0\right)_{\Gamma_{outflow}} \\
&= 0
\end{aligned}
\tag{B.2}
$$

$$\begin{aligned}
&\left(w, \frac{d\tilde{\omega}}{dt} + u_j\frac{d\tilde{\omega}}{dx_j} - \gamma\frac{\tilde{P}}{k} + \beta\omega - (\nu+\sigma_\omega\nu_T)\frac{d\tilde{\omega}}{dx_j}\frac{d\tilde{\omega}}{dx_j} - \frac{\sigma_d}{\omega}max\left(\frac{d\tilde{\omega}}{dx_j}\frac{dk}{dx_j}, 0\right)\right)_\Omega + \left(\frac{dw}{dx_j}, (\nu+\sigma_\omega\nu_T)\frac{d\tilde{\omega}}{dx_j}\right)_\Omega \\
&+\left(\tau u_j\frac{dw}{dx_j}, u_j\frac{d\tilde{\omega}}{dx_j} - \gamma\frac{\tilde{P}}{k} + \beta\omega - (\nu+\sigma_\omega\nu_T)\frac{d\tilde{\omega}}{dx_j}\frac{d\tilde{\omega}}{dx_j} - \frac{\sigma_d}{\omega}max\left(\frac{d\tilde{\omega}}{dx_j}\frac{dk}{dx_j}, 0\right)\right)_\Omega + \left(\frac{dw}{dx_j}, \nu_{DC,\omega}\frac{d\tilde{\omega}}{dx_j}\right)_\Omega \\
&-\left(w, (\nu+\sigma_\omega\nu_T)n_j\frac{d\tilde{\omega}}{dx_j}\right)_{\Gamma_{wall}} - \left(\frac{dw}{dx_j}, (\nu+\sigma_\omega\nu_T)n_j(\tilde{\omega}-g_k)\right)_{\Gamma_{wall}} + (C_b w, \tilde{\omega}-g_k)_{\Gamma_{wall}} \\
&-\left(w, u_j n_j(\tilde{\omega}-\tilde{\omega}_\infty)\right)_{\Gamma_{backflow}} \\
&-(w,0)_{\Gamma_{outflow}} \\
&=0
\end{aligned} \tag{B.3}$$

$$k = k_0 e^{\tilde{k}} \tag{B.4}$$

$$\omega = \omega_0 e^{\tilde{\omega}} \tag{B.5}$$

$$\tilde{P} = \min(P, 10\beta^* k\omega) \tag{B.6}$$

$$\tau = \left(u_i G_{ij} u_j + 12\nu^2 G_{ij} G_{ij}\right)^{-\frac{1}{2}} \tag{B.7}$$

$$C_b = \frac{4(p+1)^2\nu}{h} = 4(p+1)^2\nu\sqrt{n_i G_{ij} n_j} \tag{B.8}$$

$$\nu_{DC} = \frac{1}{G_{ii}} C_{rb}|R| \tag{B.9}$$

References

Abe, K. I., Jang, Y. J., & Leschziner, M. A. (2003). An investigation of wall-anisotropy expressions and length-scale equations for non-linear eddy-viscosity models. *International Journal of Heat and Fluid Flow*, *24*, 181–198. https://doi.org/10.1016/S0142-727X(02)00237-0

Abe, K. I., Kondoh, T., & Nagano, Y. (1997). On reynolds-stress expressions and near-wall scaling parameters for predicting wall and homogeneous turbulent shear flows. *International Journal of Heat and Fluid Flow*, *18*, 266–282. https://doi.org/10.1016/S0142-727X(97)00008-8

Allmaras, S. R., Johnson, F. T., & Spalart, P. R. (2012). Modifications and clarifications for the implementation of the spalart-allmaras turbulence model. *7th International Conference on Computational Fluid Dynamics, ICCFD 2012*, 9–13.

Apsley, D. D., Chen, W. L., Leschziner, M. A., & Lien, F. S. (1997). Non-linear eddy-viscosity modelling of separated flows. *Journal of Hydraulic Research*, *35*, 723–748. https://doi.org/10.1080/00221689709498386

Apsley, D. D., & Leschziner, M. A. (1998). A new low-reynolds-number nonlinear two-equation turbulence model for complex flows. *International Journal of Heat and Fluid Flow*, *19*, 209–222. https://doi.org/10.1016/S0142-727X(97)10007-8

Apsley, D. D., & Leschziner, M. A. (2000). Advanced turbulence modelling of separated flow in a diffuser. *Flow, Turbulence and Combustion*, *63*, 81–112. https://doi.org/10.1023/a:1009930107544

Bassi, F., Crivellini, A., Rebay, S., & Savini, M. (2005). Discontinuous galerkin solution of the reynolds-averaged navier-stokes and k-ω turbulence model equations. *Computers and Fluids*, *34*, 507–540. https://doi.org/10.1016/j.compfluid.2003.08.004

Bazilevs, Y., & Hughes, T. J. R. (2007). Weak imposition of dirichlet boundary conditions in fluid mechanics. *Computers and Fluids*, *36*, 12–26. https://doi.org/10.1016/j.compfluid.2005.07.012

Bazilevs, Y., Michler, C., Calo, V. M., & Hughes, T. J. (2007). Weak dirichlet boundary conditions for wall-bounded turbulent flows. *Computer Methods in Applied Mechanics and Engineering*, *196*, 4853–4862. https://doi.org/10.1016/j.cma.2007.06.026

Brooks, A. N., & Hughes, T. J. R. (1982). Streamline upwind/petrov-galerkin formulations for convection dominated flows with particular emphasis on the incompressible navier-stokes equations. *Computer Methods in Applied Mechanics and Engineering*, *32*, 199–259. https://doi.org/10.1016/0045-7825(82)90071-8

Carlson, J. R., Duquesne, N., Rumsey, C. L., & Gatski, T. B. (2001). Computation of turbulent wake flows in variable pressure gradient. *Computers and Fluids*, *30*, 161–187. https://doi.org/10.1016/S0045-7930(00)00007-4

Codina, R., & Soto, O. (1999). Finite element implementation of two-equation and algebraic stress turbulence models for steady incompressible flows. *International Journal for Numerical Methods in Fluids*, *30*, 309–333. https://doi.org/10.1002/(SICI)1097-0363(19990615)30:3<309::AID-FLD844>3.0.CO;2-J

Durbin, P. A., & Reif, B. A. (2010). *Statistical theory and modeling for turbulent flows* (2nd). John Wiley & Sons, Ltd. https://doi.org/10.1002/9780470972076

Franca, L. P., & Hughes, T. J. R. (1993). Convergence analyses of galerkin least-squares methods for symmetric advective-diffusive forms of the stokes and incompressible navier-stokes equations. *Computer Methods in Applied Mechanics and Engineering*, *105*, 285–298. https://doi.org/10.1016/0045-7825(93)90126-I

Franke, M., Wallin, S., & Thiele, F. (2005). Assessment of explicit algebraic reynolds-stress turbulence models in aerodynamic computations. *Aerospace Science and Technology*, *9*, 573–581. https://doi.org/10.1016/j.ast.2005.06.002

Fries, T., & Matthies, H. G. (2004). *A review of petrov-galerkin stabilization approaches and an extension to meshfree methods*.

Gatski, T. B., & Jongen, T. (2000). Nonlinear eddy viscosity and algebraic stress models for solving complex turbulent flows. *Progress in Aerospace Sciences*, *36*, 655–682. https://doi.org/10.1016/S0376-0421(00)00012-9

Gatski, T. B., & Speziale, C. G. (1993). On explicit algebraic stress models for complex turbulent flows. *Journal of Fluid Mechanics*, *254*, 59–78. https://doi.org/10.1017/S0022112093002034

Hellsten, A. (2005). New advanced k-ω turbulence model for high-lift aerodynamics [Based on Menter's k-omega SST model. The constitutive model, i.e. the additional stress anisotropy model is Wallin &; Johansson 's.

It essentially recalibrates Menter's model for use with EARSM.]. *AIAA Journal*, *43*, 1857–1869. https://doi.org/10.2514/1.13754

Hellsten, A., & Wallin, S. (2009). Explicit algebraic reynolds stress and non-linear eddy-viscosity models. *International Journal of Computational Fluid Dynamics*, *23*. https://doi.org/10.1080/10618560902776828

Hughes, T. J. R., Cottrell, J. A., & Bazilevs, Y. (2005). Isogeometric analysis: Cad, finite elements, nurbs, exact geometry and mesh refinement. *Computer Methods in Applied Mechanics and Engineering*, *194*, 4135–4195. https://doi.org/10.1016/j.cma.2004.10.008

Hughes, T. J. R., Franca, L. P., & Hulbert, G. M. (1989). A new finite element formulation for computational fluid dynamics: Viii. the galerkin/least-squares method for advective-diffusive equations. *Computer Methods in Applied Mechanics and Engineering*, *73*, 173–189. https://doi.org/10.1016/0045-7825(89)90111-4

Hughes, T. J. R., & Mallet, M. (1986). A new finite element formulation for computational fluid dynamics: Iii. the generalized streamline operator for multidimensional advective-diffusive systems. *Computer Methods in Applied Mechanics and Engineering*, *58*, 305–328.

Hughes, T. J. R., Mallet, M., & Akira, M. (1986). A new finite element formulation for computational fluid dynamics: Ii. beyond supg. *Computer Methods in Applied Mechanics and Engineering*, *54*, 341–355. https://doi.org/10.1016/0045-7825(86)90110-6

Ilinca, F., & Pelletier, D. (1998). Positivity preservation and adaptive solution for the k-□ model of turbulence. *AIAA Journal*, *36*, 44–50. https://doi.org/10.2514/2.350

Jang, Y. J., Leschziner, M. A., Abe, K., & Temmerman, L. (2002). Investigation of anisotropy-resolving turbulence models by reference to highly-resolved les data for separated flow. *Flow, Turbulence and Combustion*, *69*, 161–203. https://doi.org/10.1023/A:1024764307706

Lien, F. S., & Leschziner, M. A. (1994). Assessment of turbulence-transport models including non-linear rng eddy-viscosity formulation and second-moment closure for flow over a backward-facing step. *Computers and Fluids*, *23*, 983–1004. https://doi.org/10.1016/0045-7930(94)90001-9

Menter, F. R., Kuntz, M., & Langtry, R. (2003). Ten years of industrial experience with the sst turbulence model turbulence heat and mass transfer. *Cfd.Spbstu.Ru*, *4*, 625–632. https://cfd.spbstu.ru/agarbaruk/doc/2003_Menter,%20Kuntz,%20Langtry_Ten%20years%20of%20industrial%20experience%20with%20the%20SST%20turbulence%20model.pdf%0Ahttp://cfd.mace.manchester.ac.uk/flomania/pds_papers/file_pds-1068134610Menter-SST-paper.pdf

Nieuwstadt, F. T. M., Westerweel, J., & Boersma, B. J. (2016). *Turbulence: Introduction to theory and applications of turbulent flows*. https://books.google.com/books?hl=nl&lr=&id=zDylDAAAQBAJ&oi=fnd&pg=PR9&dq=turbulence+nieuwstadt&ots=ry8DgXlhBR&sig=OCFl7pL-rILduPUv2MMSs-wow7Y

Piegl, L., & Tiller, W. (1997). *The nurbs book*.

Pope, S. B. (1975). A more general effective-viscosity hypothesis. *Journal of Fluid Mechanics*, *72*, 331. https://doi.org/10.1017/S0022112075003382

Pope, S. B. (2000). *Turbulent flows*. Cambridge University Press. https://doi.org/10.1017/CBO9780511840531

Rijkens, A. A., Cleijsen, H. M., & Keuning, J. A. (2013). On the hydrodynamic performance of an improved motion control device for fast ships. *FAST 2013 - 12th International Conference on Fast Sea Transportation*.

Rijkens, A. A., Keuning, J. A., & Huijsmans, R. H. (2011). A computational tool for the design of ride control systems for fast planing vessels. *International Shipbuilding Progress*, *58*, 165–190. https://doi.org/10.3233/ISP-2012-0074

Rodi, W. (1976). A new algebraic relation for calculating the reynolds stresses. *ZAMM - Journal of Applied Mathematics and Mechanics / Zeitschrift für Angewandte Mathematik und Mechanik*, *56*. https://doi.org/10.1002/zamm.19765613093

Shakib, F., Hughes, T. J., & Johan, Z. (1991). A new finite element formulation for computational fluid dynamics: X. the compressible euler and navier-stokes equations. *Computer Methods in Applied Mechanics and Engineering*, *89*, 141–219. https://doi.org/10.1016/0045-7825(91)90041-4

Spencer, A. J., & Rivlin, R. S. (1958). The theory of matrix polynomials and its application to the mechanics of isotropic continua. *Archive for Rational Mechanics and Analysis*, *2*, 309–336. https://doi.org/10.1007/BF00277933

Stefanski, D. L., Glasby, R. S., Erwin, J. T., Allmaras, S. R., Coder, J. G., & Burgessn, N. K. (2018). A modified k-ω turbulence model for finite-element cfd. *2018 Fluid Dynamics Conference*. https://doi.org/10.2514/6.2018-4041

Wallin, S., & Johansson, A. V. (2000). An explicit algebraic reynolds stress model for incompressible and compressible turbulent flows. *Journal of Fluid Mechanics*, *403*, 89–132. https://doi.org/10.1017/S0022112099007004

Wang, C., Jang, Y. J., & Leschziner, M. A. (2004). Modelling two- and three-dimensional separation from curved surfaces with anisotropy-resolving turbulence closures. *International Journal of Heat and Fluid Flow*, *25*, 499–512. https://doi.org/10.1016/j.ijheatfluidflow.2004.02.009

Wilcox, D. C. (1988). Reassessment of the scale-determining equation for advanced turbulence models. *AIAA Journal*, *26*, 1299–1310. https://doi.org/10.2514/3.10041